Paleoceanography of the Barents Sea continental margin, north of Nordaustlandet, Svalbard during the last 74 ka

TEENA CHAUHAN, TINE L. RASMUSSEN AND RIKO NOORMETS

We have investigated gravity core HH11-09GC from 488 m water depth at the northern Svalbard margin in order to reconstruct changes in Atlantic Water (AW) inflow to the Arctic Ocean. The study is based on the distribution patterns of benthic and planktic foraminifera, benthic and planktic oxygen and carbon isotopes, lithology and physical properties of the sediments. The core contains sediments from Marine Isotope Stage (MIS) 5a to 1. MIS 4 was characterised by glacial conditions with advance of the Svalbard-Barents Sea Ice Sheet (SBIS) at c. 65 ka and formation of a polynya in front of the SBIS at c. 62 ka. During late MIS 3 (32–29 ka) and MIS 2 (22–20 ka), strong influence of AW resulted in high productivity of both planktic and benthic foraminiferal faunas. During 23–22 ka, the SBIS advanced to the shelf edge. The last deglaciation began at 18.5 ka and at 16.9 ka 'a maximum' in influx of meltwater from the retreating SBIS caused a weakening of the ocean circulation. At the start of the Bølling-Allerød interstadial c. 15.5 ka, inflow of relatively warm AW probably intensified the release of meltwater at 14 ka and 12.8 ka. This probably led to expansion of sea-ice cover during the Younger Dryas stadial. The late Holocene from 3.7 ka was characterised by presence of seasonal to perennial sea-ice cover and a slight warming of the bottom waters. The sea-ice cover decreased for a short period at 1.5 ka due to the advection of relatively warm AW. Correlation with results from the north-western Svalbard margin shows that the patterns of ice retreat and advance

correlate closely with changes in inflow of AW and were regulated by meltwater discharge, sea-ice export and insolation.

Teena Chauhan (teena.chauhan@unis.no, chauhan2081@gmail.com), Department of Arctic Geology, The University Centre in Svalbard (UNIS), N-9171 Longyearbyen, Svalbard, Norway and Department of Geology, UiT-The Arctic University of Norway, NO-9037 Tromsø, Norway; Tine. L. Rasmussen, CAGE - Centre for Arctic Gas Hydrate, Environment and Climate, Department of Geology, UiT-The Arctic University of Norway, NO-9037 Tromsø, Norway; Riko Noormets, Department of Arctic Geology, The University Centre in Svalbard (UNIS), N-9171 Longyearbyen, Svalbard, Norway

Keywords: Foraminifera, Arctic Ocean, Atlantic Water, Bottom water temperatures, Svalbard-Barents Sea Ice Sheet

Warm and saline Atlantic surface water derived from the Gulf Stream in the North Atlantic Ocean flows northward through the Nordic Seas and into the Arctic Ocean. Variations in this inflow of Atlantic Water (AW) are considered an integral element in regulating regional as well as global climatic conditions. Studies show that AW inflow has a direct impact on sea-ice distribution in the Arctic Ocean (Rippeth *et al.* 2015). In the marginal areas of the Arctic Ocean, such as the Barents Sea, the Kara Sea and the north-eastern Nordic Seas, the temperature and salinity of the AW and sea-ice export from the Siberian shelves determine the balance between thickness of the Polar Water and fresh meltwater layers at the surface, and the relatively saline subsurface AW. Furthermore, strength of the thermohaline circulation is also a function of high latitude cooling, and freshwater and sea-ice export from the Arctic Ocean. Hence, the properties of the AW control the distribution of sea-ice in the marginal areas of the Arctic Ocean and have a profound effect on the global thermohaline circulation.

In the northern part of the Fram Strait, the AW submerges beneath the surface Polar Water and flows as subsurface water mass between 100 m and 600 m water depth (Rudels *et al.* 2011). This water mass is called the Svalbard Branch, as it branches off the West Spitsbergen Current, which flows along the northern Svalbard margin (Rudels *et al.* 2011) (Fig. 1). Recent studies from north of Svalbard show c. 10% sea-ice loss with 0.3 °C warming of the AW per decade with high rates of sea-ice retreat during winter (Onarheim *et al.* 2014). This oceanic warming has caused retreat of the ice edge along the pathway of the inflowing AW. Previous investigations from this area have either focused on long sedimentary records from the lower slope at the northern Barents Sea margin covering the last 145 ka (Knies & Stein 1998; Knies *et al.* 2000; Wollenburg *et al.* 2001) or on short records from the shelf at Hinlopen Trough covering the last deglaciation and the Holocene periods (Koç *et al.* 2002; Ślubowska *et al.* 2005) (Fig. 1). Yet, the glacial history of AW inflow to the Arctic Ocean and the paleoceanography of the upper slope north of Nordaustlandet are poorly known. The northern Svalbard margin is, therefore, of particular interest to understand the variability of AW inflow during the last glacial-interglacial period.

For this study, a sediment core HH11-09GC was obtained from the upper slope north of Nordaustlandet from 488 m water depth. Presently, the core site is influenced by seasonal sea-ice cover and high productivity (Wollenburg & Kuhnt 2000). We investigated the strength and variation of the flow of subsurface AW during the past c. 74 ka using the distribution of planktic and benthic foraminiferal faunas as well as benthic and planktic stable isotopes. In addition, lithological parameters including concentration of ice-rafted debris (IRD) and bottom water temperature estimations based on benthic foraminifera-derived transfer functions are used for environmental reconstruction. Our results from the northern Svalbard margin are compared with data from the southern Yermak Plateau (Chauhan *et al.* 2014) to study the effect of AW inflow on sediments along the north-western and northern Svalbard margin.

Oceanographic setting

AW enters the Fram Strait at the surface (T> 2 °C and S > 35 psu; Hopkins *et al.* 1991) as the West Spitsbergen Current, which is a continuation of the North Atlantic Current (Fig. 1). At the northern part of the Fram Strait, the AW submerges under the icy and cold Polar Water of the Arctic Ocean and flows as a subsurface water mass (T = 0–2 °C and S = 34.7–35 psu; Slubowska *et al.* 2005) north of Svalbard (Rudels *et al.* 2011; Fig. 1). Around 80°N, the West Spitsbergen Current splits into two branches: the Svalbard Branch, which turns eastward and flows along the northern Svalbard margin, and the Yermak Branch, which flows northwards following the topography of the Yermak Plateau (Rudels *et al.* 2011). The Svalbard Branch is relatively warmer and saltier than the Yermak Branch. Cold Polar Water of the East Greenland Current originating from the Siberian shelves flows southward along the eastern Greenland margin into the North Atlantic Ocean (Fig. 1).

The upper water masses of the Arctic Ocean are characterised by Polar Water (T = 0–1.7 °C and S < 34.4 psu) and Arctic Water (T< 0 °C and 34.4 ≤ S ≤ 34.9 psu). Below the Polar and Arctic Water layers the AW (T = 0–2.5 °C and S>34.9 psu) is extending to the bottom of the shelf and upper slope. The main flow of the AW occurs between 100 m and 600 m water depths. In the deeper waters below the AW, relatively cold Lower Arctic Intermediate Water (T< 0 °C and S ≥34.9 psu) is found (Rudels *et al*. 2011). The salinity and temperature profiles collected at the HH11-09GC core site in September 2011 show that the 10 m thick mixed surface layer was underlain by Polar Water from 10–30 m (T = < 2 °C and S = 33.5–34.4 psu) and Arctic Water from 30–110 m (T = 2.2–3.6 °C and S = 34.4–34.9 psu) (Fig. 2). In the lower part, from 75–110 m water depth, the water mass was relatively cold and less saline probably due to the influence of glacial meltwater (T = 2.2 °C and S = 34.8 psu). The AW was found between 110 m and 488 m with a salinity of 35.05 psu, but with a gradually decreasing temperature with depth from 3.6 °C to 2.2 °C (Fig. 2).

Material and methods

A 466 cm long gravity core HH11-09GC was recovered from a water depth of 488 m north of Nordaustlandet at 81°16´N 26°13´E during a cruise with R/V "*Helmer Hanssen*" in September 2011 (Fig. 1). In addition, 30 cm of undisturbed sediment was retrieved from the core cutter and core catcher.

The core was split and described for visible changes in colour, texture, sedimentary structures and grain size. Magnetic susceptibility was measured at 1 cm intervals using a Bartington MS2 point sensor. To investigate the colour of the sediment, the sediment surface was measured with a Colortron Spectrophotometer (Andrews & Freeman 1996). The measurements were taken at 1 cm intervals.

Based on changes in lithology, 115 samples were taken in c. 1 cm thick slices for foraminiferal and IRD analyses at 5, 2 or 1 cm intervals. Two additional samples were taken from the centre of the core cutter and core catcher, respectively. The methods for foraminifera and IRD studies are described by Chauhan *et al*. (2014). The wet samples were weighed and dried in an oven at 40°C. The dried samples were weighed again and the water content was calculated. Porosity and Dry bulk density were calculated using the formulas:

Porosity = Water content /volume *(1)*

Dry bulk density = Wet bulk density - (1.026*(Porosity/100)) *(2)*

where Wet bulk density = Wet sediment weight /volume (volume = 39.28 cm^3)

Using the 63 µm, 100 µm and 1 mm stacked sieves, the sediment samples were wet sieved and residues were dried. Up to 300 planktic and 300 benthic specimens were picked from the residues of the size fraction 100 µm–1 mm. Samples with less than 50 specimens were not considered for interpretation, but were noted as barren intervals. From the picked planktic species, numbers of specimens of *Neogloboquadrina pachyderma* (sinistral) (hereafter referred to as *N. pachyderma* (Darling *et al*. 2006)) and *Turborotalita quinqueloba* were counted. All benthic species were identified to species level. The relative abundance (in %) of identified planktic and benthic species were calculated in relation to total counts of each. The concentrations of planktic and benthic foraminifera were calculated as number of foraminifera per gram dry weight sediment (no./g). Using these two concentrations, the planktic/benthic (P/B) ratio was calculated. Planktic and benthic foraminiferal flux (no. $cm^{-2}ka^{-1}$) were calculated using the formula:

Flux = Concentration of foraminifera (no./g) x Mass accumulation rate (MAR) *(3)*

where MAR (g $cm^{-2}ka^{-1}$) = Linear sedimentation rate (cm/ka) x Dry bulk density (g/cm^3)

The residue of the 100 µm–1mm size fraction was then dry sieved using 150 µm and 500 µm sieves for the counts of lithic grains to study IRD. 250–300 lithic grains were counted from each sample and subdivided into three size fractions to calculate concentrations of IRD (number of grains per 1 g of dry weight sediment). The different size fractions of IRD were categorised as coarse-grained IRD (> 1mm), medium-grained IRD (0.5–1 mm) and fine-grained IRD (0.15–0.50 mm).

Scanning electron micrographs and elemental composition images of foraminifera were taken with a Hitachi TM3000 Scanning Electron Microscope (SEM) integrated with Quantax 70

Energy Dispersive Spectroscopy (EDS) System at the Department of Geology, University of Tromsø, Norway (Figs 3A, B, C).

Eleven foraminiferal samples were analysed using Accelerator Mass Spectrometry (AMS-^{14}C) at the Radiocarbon Dating Laboratory of Lund University, Sweden and four bivalve shell samples at the Ångström Radiocarbon Laboratory of Uppsala University, Sweden. Conventional ages were calibrated to calendar ages using the Calib 7.02 calibration software and Marine13 Radiocarbon Age calibration curve. Since the present difference in reservoir age is small compared to the uncertainty of the dating, we decided to apply only an integrated standard reservoir correction (-405 years) (Stuiver & Reimer 1993; Reimer *et al.* 2013). Calibrated age range with 1 sigma standard deviation (68.3%) is used and the mid-point of ±1σ age range was calculated. Three calendar ages from bivalves and one age from benthic foraminiferal species were not used due to age reversals, in addition to, two infinite ages from samples at 380 cm and 411 cm core depth (Table 1). The ages were obtained from the planktic foraminiferal species *N. pachyderma*, the benthic foraminiferal species *Cibicides lobatulus* and *Nonionellina labradorica*, mixed benthic foraminifers, mixed planktic foraminifers and bivalves (Table 1). Three new foraminiferal samples (mixed benthic specimens) from previously published core JM10-02GC (Chauhan *et al*. 2014) were analysed at the Radiocarbon Dating Laboratory of Lund University, Sweden to further update the age model of this record (Table 1). One age was discarded due to age reversal.

Oxygen and carbon isotope analyses from square shaped, four chambered specimens with (test size 150–250 µm) of *N. pachyderma* and specimens of the benthic foraminiferal species *Cassidulina neoteretis, Melonis barleeanus, C. lobatulus* and *Islandiella norcrossi* were performed at the Stable Isotope Laboratory, Stockholm University, Sweden. These species were particularly selected due to their continuous presence and good preservation in the samples (Fig.

3A). Benthic δ^{18}O values from *C. lobatulus, M. barleeanus* and *C. neoteretis* were corrected for isotopic disequilibrium by +0.64, +0.4 and +0.16 ‰, respectively (Duplessy *et al.* 1980; Poole *et al.* 1994). The offset of *I. norcrossi* is uncertain and therefore this was not corrected (Ślubowska-Woldengen *et al.* 2007).

Absolute bottom water temperatures were calculated using a transfer function based on the benthic foraminiferal assemblages using the C2 program (Juggins 2007). Calculations were based on the database by Sejrup *et al.* (2004) with the addition of new data from the Barents Sea by Saher *et al*. (2009). The Weighted Averaging Partial Least-Squares (WAPLS) method and 1-component were used following the recommendations by Sejrup *et al.* (2004). In this study, similar calculations using the same methods were also performed on the published benthic foraminiferal assemblage data from the southern Yermak Plateau (Chauhan *et al.* 2014) and are used for regional correlation.

Results

Sedimentology

The sediments in the middle and lower part of the core consist mainly of silt with scattered drop-stones and shell fragments of bivalves (Fig. 4). Thin sections of clay deposits could be identified from 290–280 cm and 230–220 cm core depth. Three intervals from 420–410 cm, 308–307 cm and 265–230 cm core depth are dominated by silty sand (Fig. 4). In the upper part of the core, two layers rich in sponge spicules occur from 60–50 cm and 8–4 cm core depth, respectively (Figs 3B, 4). The colour of the sediment is greenish brown except from 422–390 cm and 270–265 cm core depth, where the sediment is grey and from 20–10 cm core depth where the sediment is dark brown (Fig. 4). Brown colour of Arctic sediments is mainly due to manganese hydroxide and represents interglacial/interstadial intervals (März *et al.* 2011), whereas grey colour is typically related to glacial or deglacial phases (Polyak *et al.* 2013). Fine yellow laminae at thin intervals around 425 cm, 360 cm and 100 cm core depth correlate with red colour peaks in the spectrophotometric measurements (Fig. 4).

Magnetic susceptibility is generally low and ranges between 15 and 50 10^{-6} SI (Fig. 4), typical for the Svalbard margin (Jessen *et al.* 2010). The bottom part of the core shows relatively low and stable values, whereas the upper 220 cm reveal high and fluctuating magnetic susceptibility values. Maximum magnetic susceptibility values occur between 180 and 140 cm core depth (40–50 SI 10^{-6}) (Fig. 4).

Age Model

The age-depth model for the core HH11-09GC is based on both calibrated radiocarbon ages and on Marine Isotope Stage (MIS) boundaries defined by Martinson *et al.* (1987), assuming linear sedimentation rate changes between dated levels (Fig. 5). The calibrated radiocarbon ages between 31.8 ka and 1.5 ka indicate that the core section above 335 cm covers the time period from MIS 3–1 (Table 1). At the base of the core, the benthic stratigraphic marker species for MIS 5a *Pullenia bulloides* (e.g. Haake & Pflaumann 1989; Fronval & Jansen 1997), could be identified (Fig. 6; Table 2). Therefore, a tentative age of c. 74 ka was assigned to the base of the core. The MIS 5/4 transition (c. 71 ka) is defined by increase in the planktic and benthic δ^{18}O values to 4.3‰ and 4.5‰, respectively together with a change in sediment colour from brown to grey (Figs 4, 7). The MIS 4/3 boundary (c. 60 ka) is defined from 405–400 cm core depth based on a decline of planktic δ^{18}O values to 3.5‰ in combination with a gradual change in sediment colour from grey to brown (Figs 4, 7). The low $\delta^{18}O$ values correlate with the presence of benthic foraminiferal species termed 'Atlantic species', which are characteristic of Heinrich event H6 (c. 60 ka) (cf. Rasmussen *et al.* 2014a) (Figs 6, 7). The MIS 3/2 boundary (c. 28 ka) is defined at 280 cm core depth, where the planktic $\delta^{18}O$ values show gradual increase after 29.4 ka at 285 cm core depth (Fig. 7). Similarly, after 11.9 ka at 75 cm core depth, the sediment colour changes from lighter brown (10YR 5/2) to dark brown (5YR 4/2). This transition defines the MIS 2/1 boundary (c.11.7 ka) at 70 cm core depth (Fig. 4).

Faunal distribution

The dominant planktic foraminiferal species in the core is *N. pachyderma* (c. 20–99%) followed by *T. quinqueloba* (c. 1–84%). A total of 44 benthic foraminiferal species have been identified. The 12 most abundant benthic species are *C. neoteretis* (15–60%), *M. barleeanus* (10–50 %), *C. lobatulus* and *Astrononion gallowayi* (5–25%), *I. norcrossi* (10–40 %), *Buccella* spp. (5–40%), *Cassidulina reniforme* (10–40%), *N. labradorica* (2–15%), *Elphidium excavatum* and *Elphidium* spp. (25–50%) and *P. bulloides* (0–12%) (Figs 3A, 6). The concentration of benthic foraminifera was high during late MIS 4, late MIS 3 and during the last glacial maximum (LGM) in MIS 2 (Fig. 4). The flux of planktic species and the P/B ratio was remarkably high during the LGM (Figs 4, 6).

A group of subtropical-boreal benthic species ('Atlantic species', cf. Rasmussen and Thomsen, 2004) are present at certain intervals in the core (Fig. 3C). These species include: *Anomalinoides minimus, Cibicides pachyderma, Eggerella bradyi, Eilohedra nipponica, Gyroidina umbonata*, *Pyrgo* sp., *Marginulinopsis costata, Cornuloculina inconstans, Pullenia subcarinata, Pyrgo williamsoni, Pyrgoella irregularis, Robertinoides* sp., *Sagrina subspinescens,* *Sphaeroidina bulloides, Triloculina oblonga and Valvulineria arctica.* This group constitutes 0–10% of the benthic assemblage (Fig. 6). The 'Atlantic species' have also been identified in core JM10-02GC from the southern Yermak Plateau, where they constitute up to 6% of the benthic fauna (Chauhan *et al.* 2014). Based on the abundance of 'Atlantic species' and the criteria suggested by Rasmussen *et al.* (2014a), six intervals in HH11-09GC and JM10-02GC cores have been correlated with Heinrich events H6–H1 between MIS 4 and MIS 2 (Fig. 8). Similarly, using this new data set, the age model of core JM10-02GC was slightly revised, and boundaries of MIS 5/4 (c. 71 ka) and MIS 4/3 (c. 60 ka) are now defined at 265 cm and 300 cm core depth, respectively. These revised core depths and two new dates in core JM10-02GC (Table 1) were used for conversion of the depth scale to age scale.

In the late Holocene section, eleven species of agglutinated foraminifera could be identified from 18–1 cm core depth. These are *Cribrostomoides crassimargo, Centropyxis arenatus, Glomospira charoides, Rhabdammina abyssorum, Rhabdammina* sp., *Reophax micacea, Rheophax* sp., *Rhizammina indivisa, Saccammina difflugiformis, Trochammina orchracea and Trochammina* spp. The percentage of agglutinated specimens to total benthic foraminifera counts ranged between 30% and 60%.

Concentration of IRD

Relatively high concentration of coarse-grained (>1 mm) and medium-sized IRD (0.5–1 mm) occurs at the transitions to glacial and interglacial periods, except for the MIS 3/2 transition (Fig. 4). The highest concentrations of coarse- and medium-sized IRD correlate with the MIS 2/1 transition. The concentration of fine-grained IRD (0.15–0.50 mm) is moderate in these intervals. The highest concentration of fine-grained IRD occurs at c. 30.5 ka (308–307 cm core depth) in

MIS 3 and at 22 ka (265–230 cm core depth) in MIS 2 (Fig. 4). Due to the size of the sand grains, the sand layers/lenses is grouped under the fine-grained IRD category, even though they were not deposited as sea-ice or iceberg melt-out (for their depositional environment, see interpretation) (Fig. 4).

Planktic and benthic stable isotopes

The benthic $\delta^{18}O$ values are high in MIS 4 and MIS 2 and relatively low in MIS 5a, at 16.9 ka (220 cm core depth) during the last deglaciation, and in MIS 1 (Fig. 7). The $\delta^{13}C$ values measured in the epi-benthic species *C. lobatulus* are high in the LGM and MIS 1. The other species used for isotopic analyses are endo-benthic and show relatively low $\delta^{13}C$ values (Fig. 7). The planktic $\delta^{18}O$ values are low in Heinrich event intervals H6 (c. 60 ka), H5 (c. 48 ka) and H1 (16.9 ka), and at c. 12.8 ka (95 cm core depth) in late MIS 2 and in MIS 1(Fig. 7). The planktic $\delta^{13}C$ record show high values during the MIS 5a/4 transition period (c. 71–70 ka) and MIS 1 (3.7 ka), and variable values during MIS 3 and low values during MIS 2.

Bottom water temperature (BWT)

The BWT obtained from transfer function calculations ranges between approximately -1 ^{o}C and +1 ^{o}C (Fig. 7). These values are lower than shown in the modern CTD record (Fig. 2). The reason is that the calculated BWT is obtained from the entire benthic species assemblage (see also discussion in Rasmussen *et al*. 2014b), which represents a 100–500 years average of all seasons, whereas the modern CTD shows data from one point measurement at a specific time of the year (here autumn 2011). Today, the temperature of the AW shows a high seasonal and year-to-year variability (Svendsen et al., 2002; Dmitrenko et al., 2004; Cottier et al., 2005; Ivanov et al., 2009). The calculated trend is consistent with the variations in the $\delta^{18}O$ values measured in benthic foraminifera (Fig. 7). The BWT was mainly below 0 °C between MIS 4 and MIS 2 except for certain intervals, including Heinrich events H6, H4, H3 and H1, where BWT was above 0 °C. A minimum of -1 °C is calculated at 22 ka during the LGM. During MIS 5a, the last deglaciation period and MIS 1, relatively warm bottom waters existed. The maximum BWT of +1.2 °C was recorded in MIS 1 (Fig. 7).

Discussion

Interpretation of paleoceanographic conditions of the northern Barents Sea margin

Bottom water conditions

Throughout the record, the benthic foraminiferal species *C. neoteretis, I. norcrossi, C. reniforme, E. excavatum* and *C. lobatulus* are the most abundant species in the sediments suggesting that inflow of chilled AW and relatively strong bottom currents with seasonal sea-ice conditions have influenced the core site since c. 74 ka (Fig. 6; Table 2). To some extent, highest abundance of *M. barleeanus* is also reflecting inflow of relatively warm AW.

High flux of benthic foraminifera correlates with relatively high abundance of *I. norcrossi*, for example, at c. 62 ka in late MIS 4 (420–410 cm core depth), from 32–29 ka in late MIS 3 (340–290 cm core depth), from 22–17 ka in MIS 2 (265–225 cm core depth) (Fig. 6). This indicates that seasonally open water was present with high seasonal productivity due to presence of the sea-ice margin and seasonal sea-ice at the core site (Table 2). The open water conditions could have resulted from advection of AW and/or the formation of local polynyas by upwelling of nutrient rich AW.

C. neoteretis, indicating influence of chilled AW, flowing subsurface, is present throughout the record except for foraminiferal barren intervals (Fig. 6; Table 2). Today, *C. neoteretis* is abundant in areas with stratified water column, which may occur due to presence of meltwater at the surface or due to drifting sea-ice from the Arctic Ocean (Wollenburg & Mackensen 1998). This suggests stratified water column conditions where the AW has been flowing as subsurface water mass beneath cold and less saline Polar surface Water. *M. barleeanus* shows negative correlation with *C. neoteretis* indicating influence of relatively warm AW. This may indicate open water conditions, such as, during the interstadials following the cold Heinrich event H3 at c. 37 ka (345 cm), during Bølling-Allerød interstadial from c. 13–12 ka (120–100 cm) and during the MIS 2/1 transition at c. 11.7 ka (70 cm) (Fig. 6; Table 2).

Some intervals in MIS 4, early MIS 3 and MIS 2 show high relative abundance of *N. labradorica* (Fig. 6). *E. excavatum* is often an accompanying species in these intervals. Together, the species indicate cold, polar conditions suggesting that the Polar Front had moved southward close to the core site and that the influence of AW was weaker (low *C. neoteretis*) (Table 2). *E. excavatum* also became abundant during the late Holocene, indicating inflow of low salinity Polar Water over the upper slope at that time (Fig. 6). *Buccella* spp., which indicates high supply of food mainly at the sea-ice margin, was most abundant during the Younger Dryas/Holocene transition and in the late Holocene (Fig. 6; Table 2). Seidenkrantz (2013) proposed that different species of *Buccella* mainly respond to increased availability of food irrespective of the cause.

C. lobatulus was present during most of MIS 5a to 1, but its relative abundance was highest during the Holocene, which along with the group of 'Atlantic species' suggests strong and relatively warm bottom currents, correlating well with the calculated BWT (Figs 6, 7; Table

2). The almost 'fully interglacial' species *P. bulloides* (e.g. Haake & Pflaumann 1989; Fronval & Jansen 1997) was present at the bottom of the core and in the late Holocene sediments (Fig. 6). This species is relatively rare in glacial sediments and lives in a narrow salinity range of c. 35 psu and a temperature between 2 °C and 4 °C (Table 2).

Subsurface water conditions

N. pachyderma is the dominant planktic foraminiferal species, with the highest abundance of c. 99% during early MIS 4 and MIS 4/3 transition (Fig. 6). The sub-polar species *T. quinqueloba* shows maximum abundance of up to 84% at 23 ka in MIS 2 and during MIS 2/1 transition period (Fig. 6). The intervals with low percentage of *N. pachyderma* on the northern Svalbard margin could probably be attributed to subsurface flow of AW where *T. quinqueloba*, which is associated with productive Arctic Waters and the Arctic/Polar Fronts, became more abundant (Fig. 6; Table 2). The highest abundance of *N. pachyderma* occurred during MIS 4 and early MIS 3 suggesting strong influence of Polar Water at the surface. High relative abundance of *T. quinqueloba* indicates periods of reduced influence of Polar Water. This is observed in intervals prior to Heinrich events H6, H3, H2 and H1 and in the late Holocene (Fig. 6).

Heinrich event intervals

From MIS 4 to MIS 2, six intervals with characteristics of Heinrich events (H6–H1) in the Nordic Seas are distinguished in cores HH11-09GC and JM10-02GC (Fig. 8). In the Nordic Seas and at the western Svalbard margin, these intervals are characterised by the presence of 'Atlantic species', high P/B ratio, relatively high BWT and low planktic $\delta^{18}O$ values (Fronval *et al.* 1995;

Rasmussen *et al*. 1996a, 2007, 2014a; Rasmussen and Thomsen 2004). However, during Heinrich events in the North Atlantic Ocean, abundant IRD were deposited from melting icebergs (e.g. Heinrich 1988) and the sea surface was strongly influenced by meltwater (low planktic $\delta^{18}O$ values), resulting in reduced thermohaline circulation (Broecker 1991; Bond *et al.* 1993). This, in turn, modified oceanographic conditions at high northern latitudes.

At the northern Svalbard margin, the content of coarse- and medium-sized IRD was fairly low and the Heinrich events are mainly identified based on the presence of 'Atlantic species' (Figs 4, 6). Due to low resolution and sporadic occurrence of 'Atlantic species', H4, H3 and H2 are mainly identified based on the age model and IRD peaks (Fig. 8). Low planktic $\delta^{18}O$ values during H6, H5 and H1 indicate influence of meltwater at the surface and suggest that the water column was stratified and the AW flowed at the subsurface (Fig. 7). This probably enabled the transfer of heat and 'Atlantic species' northward into the Arctic Ocean during these intervals (see e.g. Rasmussen *et al.* 2014a).

Foraminiferal barren intervals

The sediment samples in this study mostly contain well-preserved foraminifera (Figs 3A, C). Exceptions are the barren intervals during the MIS 5a/4 transition at c. 71 ka (466–460 cm core depth), during mid-MIS 4 at c. 65 ka (440–425 cm core depth) and during the last deglaciation at c. 15.6 ka (195–185 cm core depth) and at c.12.8 ka (100–90 cm core depth) (Fig. 6). Intervals barren of planktic and benthic foraminifera in MIS 4, MIS 3 and at 15.6 ka in MIS 2 are, however, rich in IRD. This suggests that the absence of foraminifera could be due to high sedimentation rates causing high turbidity (Figs 4, 6). Another explanation for the barren intervals could be low biogenic production or dissolution of calcium carbonate (Steinsund &

Hald 1994; Hald & Steinsund 1996; Zamelczyk *et al*. 2012). Dissolution is caused by higher concentration of CO_2, which may come from remineralisation of biogenic matter or from dense brines, or from glacial meltwater (Fig. 3B). Intervals barren of only planktic foraminifera, such as during the last deglaciation between c. 15.6 ka and 12.8 ka (185–100 cm core depth), when the sedimentation rates were highest could indicate presence of highly turbid water at the surface. Such conditions have been shown to be inhospitable for planktic foraminifera (Polyak *et al.* 2013).

Ice-rafting intervals

IRD peaks during MIS 4 at c. 65 ka (430 cm core depth) were probably related to the advance of the Svalbard-Barents Sea Ice Sheet (SBIS). However, high content of coarse- and medium-sized IRD during the MIS 4/3 transition at 58 ka (400 cm core depth) and during the last deglaciation at c.15.6 ka (195–185 cm core depth) probably represents iceberg and/or sea-ice melting events during the disintegration of the SBIS (Fig. 4). Drop-stones at c. 38 ka (345 cm core depth) and 15.6 ka (195–185 cm core depth) suggest intermittent intensification of iceberg rafting (Fig. 4). The sand layers deposited at c. 30 ka (308–307 cm core depth) and at 22 ka (265–230 cm core depth) were probably associated with either slope failure and/or sediment input from the SBIS that reached the shelf edge, thus representing sediment down-slope mass-transport deposits (Fig. 4). High planktic and benthic foraminifera fluxes were recorded in the sand layers, which suggest that the sea-ice margin was probably close to the core location (Fig. 6).

Regional correlation of depositional environments and paleoceanography since MIS 5a

MIS 5a/4 transition and MIS 4

In the late part of MIS 5a, gradual increase in planktic $\delta^{18}O$ values and low concentration of *N. pachyderma* indicate that the temperatures and productivity of surface waters were low (Fig. 8). Wollenburg *et al.* (2001) noticed a similar trend in a planktic isotope record from the northern Barents Sea margin. However, increased abundance of *C. neoteretis* in core HH11-09GC implies that saline and moderately warm AW must have been present as subsurface water mass (Fig. 9). Studies of modern conditions at the western Greenland margin show that increase in subsurface warming caused increased calving and melting of icebergs from outlet glaciers in the past decades (Holland *et al.* 2008). At the MIS 5/4 transition (c. 71–70 ka), relative increase in sedimentation rate and IRD concentrations are recorded in cores JM10-02GC and HH11-09GC (Fig. 8). Similar results are presented in studies from the lower slope of northern Svalbard (Knies *et al.* 2000; 2001) and the central Arctic Ocean (Spielhagen *et al.* 2004). Vogt *et al.* (2001) suggest that IRD deposited at the Yermak Plateau reflects an advance of the SBIS during late MIS 5a. It is possible that the AW inflow caused melting of the icebergs, which were released during the ice sheet advance.

The early MIS 4 was characterised by the presence of Polar Water at the surface (high % *N. pachyderma*) and weak influence of AW at the bottom (high % *E. excavatum* and *I. norcrossi)* (Figs 8, 9; Table 2). Similar conditions were observed at the northern Svalbard margin (Knies *et al.* 1999; Wollenburg *et al.* 2001) and in the Central Arctic Ocean (Nørgaard-Pedersen *et al.* 2003). However, at the southern Yermak Plateau dominance of *M. barleeanus* suggest influence of relatively warm AW at the bottom (Fig. 9), which is in agreement with studies from the Nordic Seas, where strong influence of AW resulted in open water conditions and increased rate of evaporation that contributed to the growth of the SBIS (Hebbeln *et al.* 1998; Hald *et al.* 2001).

The growing SBIS became unstable and resulted in deposition of IRD on the upper slope north of Svalbard at c. 65 ka (Fig. 8). Knies *et al.* (2001) also correlated peaks in IRD at c. 65 ka at the lower slope of the northern Barents Sea to advance of the northern SBIS.

Following the SBIS advance, the high relative abundance of *N. pachyderma* indicates the return of cold environmental conditions (Fig. 8; Table 2). Subsequently, at c. 62 ka, increase in benthic and planktic foraminiferal flux with high relative abundance of the benthic species *C. neoteretis* and *C. reniforme* and the planktic species *N. pachyderma* in core HH11-09GC indicate increase in productivity due to strong influence of AW at the subsurface and seasonally open water conditions at the surface (Figs 8, 9; Table 2). Sand layers were deposited during this period (420–410 cm core depth) (Fig. 4). The sand could originate from melting of icebergs, down-slope processes, meltwater plumes or strong currents. However, together with high abundance of benthic foraminifera, the evidence suggests that the short-lived open water conditions occurred disrupting the ice marginal conditions. We suggest that formation of polynya and down-welling caused re-deposition and formation of sand layers. Knies *et al.* (2001) also suggested that during MIS 4 and MIS 2 at the northern Barents Sea shelf, polynyas were formed due to strong winds in front of the SBIS margin, extending from the northern Svalbard margin to the Franz Victoria Trough.

MIS 3

During the MIS 4/3 transition at c. 60 ka, the presence of 'Atlantic species', high BWT, low $\delta^{18}O$ values and high relative abundance of *N. pachyderma* indicate influence of meltwater at the surface and relatively warm AW at the bottom (Fig. 8). This period correlates with Heinrich event H6. The later part of this period was characterised by high relative abundance of *E.*

excavatum implying cold conditions (Fig. 9). At the beginning of MIS 3, the SBIS probably retreated. The relatively high concentration of IRD in core JM10-02GC indicates that numerous icebergs crossed the Yermak Plateau (Fig. 8). Subsequently at c. 51 ka, dominance of the benthic species *M. barleeanus,* with higher percentages in core JM10-02GC than in core HH11-09GC, indicate inflow of relatively warm AW. The influence was apparently stronger at the southern Yermak Plateau and probably caused rapid melting of icebergs and/or sea-ice (Fig. 9; Table 2). The study by Spielhagen *et al.* (2004) also documents the presence of warm AW in the Fram Strait at 52 ka. The period of increased inflow of AW was concurrent with the retreat of the ice sheet from the western and northern Barents Sea shelf edge (Mangerud *et al.* 1998; Jakobsson *et al.* 2014). This retreat of the SBIS is also recorded in studies from the Fram Strait, the western Svalbard margin, the southern Yermak Plateau, the northern Barents Sea and in the Central Arctic Ocean (Lloyd *et al.* 1996; Darby *et al.* 1997; Hebbeln & Wefer 1997; Nørgaard-Pedersen 1997; Knies *et al.* 2001; Chauhan *et al.* 2014).

At 37.5 ka, relatively high planktic δ^{18}O values indicate a return of cold conditions at the surface north of Svalbard with reduced influence of meltwater (Fig. 8). The BWT was high indicating influence of warm AW at the bottom (Fig. 8). The timing correlates with Heinrich event H4 of the Nordic Seas (38 ka). At the northern Svalbard margin and at the southern Yermak Plateau, the concentration of IRD increased during H4 (Figs 4, 8), indicating melting of icebergs similar to other areas in the Nordic Seas.

Between 31.8 ka and 29.4 ka, a distinct increase in the flux of planktic and benthic foraminifera is recorded (Fig. 8). This suggests favourable conditions at the surface and at the sea bottom, most likely due to increased flow of AW. However, at c. 30.5 ka, an abrupt increase in sedimentation rate and a prominent peak in IRD correspond to a sand layer in core HH11-09GC (Figs 4, 8). Similar sand layers were also deposited at the southern Yermak Plateau during the same time interval (Vogt *et al.* 2001; Chauhan *et al.* 2014). The unusually old age obtained from this sand layer (34 ka) in core HH11-09GC suggests that the sediments were re-deposited, probably by the advancing SBIS and/or slope failure (Table 1). The possible slope failure could have been related to the relatively abrupt sea level drop at c. 31–30 ka (Solomon 2007, Fig. 6.8 and references therein), which could introduce unstable conditions at the shelf edge.

MIS 2

The period between 28 ka and 23 ka was characterised by glacial conditions, with low BWT, overall low fluxes of foraminifera and high planktic and benthic $\delta^{18}O$ values (Fig. 8). High relative abundance of *I. norcrossi* and low relative abundance of *C. neoteretis* indicate weak influence of AW and expansion of seasonal sea-ice cover north of Nordaustlandet (Fig. 9). In contrast, on the southern Yermak Plateau, a relatively high percentage of *C. neoteretis* indicates stronger influence of AW at the same time (Fig. 9). Increase in advection of AW caused a northward shift of the sea-ice margin to 81°N at the northern Yermak Plateau (Nørgaard-Pedersen *et al.* 2003; Müller *et al.* 2009). Several studies from the Nordic Seas and the southern Yermak Plateau show that strong advection of AW between 28 ka and 21 ka resulted in high productivity and open water conditions (Hebbeln *et al.* 1994; Dokken & Hald 1996; Hebbeln & Wefer 1997; Hald *et al.* 2001; Vogt *et al.* 2001; Nørgaard-Pedersen *et al.* 2003; Spielhagen *et al.* 2004; Chauhan *et al.* 2014). Differences in inflow of AW to the western and northern Svalbard margin most likely resulted from two key elements - the atmospheric circulation and the thickness of the halocline.

Following the period of seasonal sea-ice cover, the planktic foraminifera flux increased abruptly around 23–22 ka suggesting open water conditions (Fig. 8). This period correlated in time with Heinrich event H2. Together with the high foraminifera flux, a 20 cm thick sand layer was deposited (Fig. 8). An old age (32 ka) from the dated bivalve shell fragments indicates that the sediments are reworked (Table 1). The most likely reason for the sand deposit is the advance of the SBIS to the shelf break north of Nordaustlandet, which caused deposition of sub-glacial sediments at the core site through gravity-driven processes. The period of the SBIS advance to the northern margin correlated in time with advance of the ice sheet in the southern Svalbard shelf as well as the western Svalbard margin between 24 ka and 23 ka (Vogt *et al.* 2001; Jessen *et al.* 2010).

The last deglaciation

At 18.5 ka, the planktic and benthic $\delta^{18}O$ values started to decrease simultaneously with the rise of BWT indicating influence of meltwater at the surface and warming of the bottom waters (Fig. 8). This period marks the initiation of the last deglaciation at the upper slope north of Nordaustlandet. Clark *et al.* (2009) hypothesised that the onset of the last deglaciation in the northern hemisphere was marked by a series of meltwater events beginning at c. 19 ka. Nørgaard-Pedersen *et al.* (2003) documented decreasing planktic $\delta^{18}O$ values in the central Fram Strait, at the Yermak Plateau and in the northern Barents Sea between 18.5 ka and 16 ka. The timing was consistent with the deglaciation ages of 16.5 ka of the Svalbard margin (Lloyd *et al.* 1996), 17.7 ka in the Fram Strait (Jones & Keigwin 1988; Hebbeln *et al.* 1994), 19.1 ka at the lower slope at the northern Barents Sea margin (Knies & Stein 1998) and at 18.6 ka in the eastern Arctic Ocean (Stein *et al.* 1994).

The lowest planktic and benthic $\delta^{18}O$ values were recorded at 16.9 ka indicating freshening of the water column and weakened oceanic circulation (Fig. 8). This period correlates with Heinrich event H1, with a peak in 'Atlantic species' and increased BWT. At the southern Yermak Plateau, maximum freshening was recorded at 17.3 ka. Here, also an increase in BWT and a peak in 'Atlantic species' was noted (Figs 8, 9). Similar conditions and timing of the H1 event occur in records from the southern Svalbard margin and the western Svalbard slope (Rasmussen *et al.* 2007; Jessen *et al.* 2010). Stanford *et al.* (2011) re-defined the duration of H1 to 4000 years extending from c. 19–15 ka and recommended that this long H1 event agrees with a prolonged termination of deep water formation in the Nordic Seas.

Towards the end of H1, sedimentation rate increased and abundant IRD was released at c. 15.6 ka, probably due to disintegration of the SBIS (Fig. 8). The accumulated heat in the bottom water due to water column stratification could be the triggering mechanism for the release of icebergs (e.g. Holland *et al.* 2008; Marcott *et al*. 2011,). This period represents a dynamic phase of the last deglaciation period. Similar IRD events are recorded at 15.4 ka at the lower slope of the northern Barents Sea margin (Knies *et al.* 1999) and on the western Svalbard margin (Jessen *et al.* 2010). The absence of this IRD event at the southern Yermak Plateau indicates that the SBIS was less active on the north-western Svalbard margin than along the northern and western Svalbard margins (Fig. 8).

Following the IRD event, increase in relative abundance of *C. neoteretis* and benthic δ^{18}O values at 15.5 ka suggest advection of subsurface AW flow (Figs 8, 9). This marks the onset of the Bølling-Allerød interstadial. The period was concurrent with the continuous influx of AW to the Norwegian-Greenland Seas (Sarnthein *et al.* 1995; Hald & Aspeli 1997), to the southern Svalbard area (Rasmussen *et al.* 2007), to the western and northern Svalbard shelf (Koç *et al.* 2002; Ślubowska *et al.* 2005; Ślubowska-Woldengen *et al.* 2007; Rasmussen *et al*. 2014b) and to the Franz Victoria Trough (Lubinski *et al.* 1996). Lubinski *et al.* (2001) suggested that the deglaciation of the Kara Sea ice sheet commenced by glacio-fluvial flows, which may have influenced the core site of HH11-09GC as well (high magnetic susceptibility, planktic foraminiferal barren interval; Figs 4, 8).

During most of the Bølling-Allerød interstadial the planktic $\delta^{18}O$ values were low reflecting influence of meltwater at the surface (Fig. 8). The timing correlates with the meltwater plume recorded on the western Svalbard margin from c. 14.7–14.3 ka (Jessen *et al.* 2010). The synchronicity of these events suggests that similar oceanographic conditions were present on the western and northern Svalbard shelf as the SBIS decayed. Towards the end of the interstadial period and at the start of the Younger Dryas stadial at 12.8 ka, low planktic $\delta^{18}O$ values indicate the influence of another meltwater pulse (Fig. 8). The sediment laminae in the core at 95 cm core depth support this interpretation (Fig. 4). Evidence for a meltwater pulse during the same period has also been reported in records from the Franz Victoria and St. Anna Troughs (Lubinski *et al.* 2001) and from the Laptev Sea (Spielhagen *et al.* 2005).

The presence of fresh meltwater at the surface probably facilitated the expansion of sea-ice during the Younger Dryas stadial, as indicated by gradually increasing planktic $\delta^{18}O$ values and the re-appearance of polar planktic species *N. pachyderma* reflecting colder conditions (Fig. 8). High relative abundance of *E. excavatum* correlates with the Younger Dryas interval at the southern Yermak Plateau (Fig. 9). Sea-ice biomarker proxy records from the eastern Laptev Sea show enhanced sea-ice formation at 12.8 ka preceding the freshwater event (Fahl & Stein, 2012). The northern Barents Sea east of Nordaustlandet was covered by near-perennial sea-ice according to Kristensen *et al.* (2013), whereas in the Hinlopen Strait (Koç *et al.* 2002; Ślubowska *et al.* 2005) and on the western Svalbard margin (Ślubowska-Woldengen *et al.* 2007) seasonal sea-ice cover was present. The evidence suggests that the high rate of sea-ice formation in the Arctic was linked to freshwater input. The export of sea-ice from the Arctic could have promoted colder conditions in the lower latitude regions during the Younger Dryas.

MIS 1

At the Younger Dryas/Holocene boundary (c. 11.7 ka), the high abundance of *M. barleeanus* and *Buccella* spp. indicates influence of warm AW, which probably resulted in thinning of sea-ice and increase in productivity at the sea-ice edge (Fig. 6; Table 2). Wollenburg *et al.* (2004) show that primary productivity reached 120 g cm^{-2} yr^{-1} during the Younger Dryas/Holocene transition on the northern Barents Sea margin, which was nearly twice the modern primary productivity in the area. Based on the age model, sediments of early Holocene age are absent in both cores HH11-09GC and JM10-02GC (Fig. 8). Explanation for this may involve non-deposition or erosion due to strong bottom currents. According to Polyak and Mikhailov (1996) and Aagaard-Sørensen *et al.* (2014), the advection of AW into the Nordic Seas was stronger during the early Holocene than today. Wollenburg *et al.* (2004) linked the high abundance of 'Atlantic species' between 10 ka and 9 ka to evidence of enhanced inflow of warm AW to the northern Barents Sea margin. Subsequently, Jessen *et al.* (2010) have reported occurrence of a diatom-rich layer dated between 10.1 ka and 9.8 ka as an indicator of northward movement of the Polar Front and the first strong inflow of AW along the western Svalbard shelf. Risebrobakken *et al.* (2011) suggest that the strengthening of influx of warm AW during the early Holocene was associated with the reorganization of the Atlantic Meridional Overturning Circulation. Another hypothesis is that glacio-isostatically induced bathymetric changes may have altered the flow of the AW (Lubinski *et al.* 2001).

During the late Holocene, from 3.7 ka onwards, relatively high abundance of *Buccella* spp., *P. bulloides*, 'Atlantic species' and high BWT show influence of warm AW at the sea bottom (Figs 6, 8) and presence of near-perennial to seasonal sea-ice cover at the surface. Surface water stratification and reduced heat loss of AW to the atmosphere can explain the warming of the bottom water. The surface cooling was probably caused by increased export of Arctic sea-ice and Polar Water via the East Greenland Current in the western Fram Strait. Comparable climate scenarios are also recorded from the eastern Fram Strait (Werner *et al.* 2013), from the western and northern Svalbard shelf (Ślubowska-Woldengen *et al.* 2007), at the southern Yermak Plateau (Chauhan *et al.* 2014) and from the northern Svalbard margin (Wollenburg *et al.* 2007).

At 1.5 ka, the increasing relative abundance of *C. neoteretis* show that AW regained strength resulting in reduced sea-ice cover north of Nordaustlandet (Fig. 9; Table 2). *C. neoteretis* was also abundant in the Franz Victoria trough on the northern Barents Sea margin (Duplessy *et al.* 2001). On the western Svalbard margin, the open water conditions were maintained due to advection of AW, which supplied moisture for glacier growth during this period (Svendsen & Mangerud 1997; Müller *et al.* 2012; Werner *et al.* 2013). Short-term pulses of warm AW are also reported from the western margin of the Barents Sea based on planktic foraminiferal studies (Sarnthein *et al.* 2003) and from Kveithola Trough based on coccolith studies (Dylmer *et al.* 2013). Renewal of a similar benthic assemblage (*Buccella* spp., *P. bulloides* and 'Atlantic species') with sponge spicules and agglutinated species implies that seasonal sea-ice cover developed at the core site and that the open water conditions existed for limited time intervals, only (Figs 4, 6; Table 2).

Conclusions

This study presents for the first time a long record of paleoceanographic evolution of the of the northern Svalbard margin in the southern part of the Arctic Ocean. The reconstruction of the flow of the AW was based on the distribution patterns of planktic and benthic foraminiferal assemblages, stable isotope records and lithology.

The benthic foraminiferal species *C. neoteretis* and *C. reniforme* were dominant and indicated variable subsurface inflow of AW most of the time during the past 74 ka. *I. norcrossi* was abundant from 32–29 ka in late MIS 3 and from 22–20 ka during the last glacial maximum in MIS 2, indicating high productivity associated with the sea-ice marginal conditions at the core site. *N. pachyderma* and *T. quinqueloba* were the dominant planktic species. Overall, these assemblages show that climatic and oceanographic conditions since 74 ka evolved through the interplay of sea-ice extent and thickness, episodes of open water conditions, polynyal activity and its effect on paleo-productivity.

Six Heinrich events, H6–H1 were distinguished during MIS 4 – MIS 2. Four of these, H6, H5, H3 and H1, were similar in characteristics to the Heinrich events of the North Atlantic due to the influence of meltwater from IRD events in the North Atlantic and Nordic Seas and modified oceanographic regimes at the northern Svalbard margin.

During late MIS 5a, the surface water temperature and productivity were low, and the warmer AW flowed as subsurface water mass. The accumulated heat at the subsurface below the meltwater layer accelerated the melting of icebergs at the MIS 5/4 transition (c. 71 ka). With the onset of MIS 4, peak glacial conditions prevailed with reduced influence of subsurface AW and expansion of seasonal sea-ice cover. The moisture supply from the western Svalbard margin and cold conditions on the northern Svalbard margin caused the SBIS to grow and advance during mid-MIS 4 at c. 65 ka. Later, towards the end of MIS 4, polynya formed at the northern margin of the SBIS at c. 62 ka.

During early MIS 3, the SBIS retreated and, as a result, meltwater was present at the surface, whereas the AW continued to flow at the subsurface. Advection of the AW at c. 51 ka accelerated the melting process. At c. 38 ka, the northern Svalbard margin was dominated by cold conditions, which later ameliorated between 31.8 ka and 29.4 ka due to increased influx of AW, resulting in high accumulation rates of planktic and benthic foraminifera. The conditions deteriorated at c. 30 ka for a short period and the unstable conditions at the shelf edge caused a slope failure. At the beginning of MIS 2, the influence of AW decreased and cold conditions with low sedimentation rates dominated. Later, between 23 ka and 22 ka, the influence of AW increased and concurrently the SBIS advanced to the shelf edge depositing reworked sediments on the upper slope. This also implies that the SBIS was not grounded at the core site between MIS 4 and MIS 2.

The last deglaciation began at c. 18.5 ka resulting in relatively fresh meltwater layers at the surface. Maximum freshening of the water column occurred at 16.9 ka, correlating with the Heinrich event H1. Following the period with a thick meltwater layer at the surface, abundant IRD was released at c. 15.6 ka. This event signifies the major disintegration of the northern SBIS. At 15.5 ka, the IRD deposition decreased and the increase of AW inflow caused rapid decrease of sea-ice and glacier ice in the area. This period marks the start of the Bølling-Allerød interstadial. Two meltwater pulses were released at c. 14 ka and towards the end of the Bølling-Allerød interstadial at c. 12.8 ka, respectively. Following the meltwater events, sea-ice cover expanded during the Younger Dryas stadial at c. 12.5 ka.

During the Younger Dryas/Holocene transition (at c. 11.7 ka), the sea-ice edge was at the core site. Sediments of early Holocene age are absent in the core, which was probably associated with increased advection of the AW. The resulting strong bottom currents could have caused erosion or non-deposition of sediments north of Nordaustlandet. During the late Holocene from c. 3.7 ka onwards, cold conditions with seasonal to near-perennial sea-ice cover were prevalent with an exception at 1.5 ka, when the advection of relatively warm AW reduced the sea-ice cover for a limited time period.

Acknowledgement

The study was funded by the Research Council of Norway through a grant to T. Chauhan. The Norwegian Research School in Climate Dynamics (ResClim) is acknowledged for funding the AMS-^{14}C analysis. We thank the Captain and crew of R/V *Helmer Hanssen* for help in core and data collection during the cruise in 2011. AMS-^{14}C dates were supervised by M. Rundgren (Radiocarbon Laboratory, Lund University, Sweden) and G. Possnert (Ångström Radiocarbon Laboratory, Uppsala University, Sweden). The Stable Isotope Laboratory, Stockholm is acknowledged for stable isotope analysis. T. Dahl, Department of Geology, University of Tromsø, Norway helped with SEM images. We acknowledge E. Thomsen, Aarhus University, Denmark for calculating bottom water temperature (BWT) using transfer functions. Constructive reviews by two anonymous reviewers improved the manuscript.

Conflict of interest: The authors declare that they have no conflict of interest.

References

Aagaard-Sørensen, S., Husum, K., Hald, M., Marchitto, T. & Godtliebsen, F. 2014: Sub sea surface temperatures in the Polar North Atlantic during the Holocene: Planktic foraminiferal Mg/Ca temperature reconstructions. *The Holocene 24*, 93-103.

Andrews, J. & Freeman, W. 1996: The measurement of sediment color using the colortron spectrophotometer. *Arctic and Alpine Research*, 524–528.

Bé, A. & Tolderlund, D. 1971: Distribution and ecology of living planktonic foraminifera in surface waters of the Atlantic and Indian Oceans. *The Micropaleontology of Oceans*, Cambridge University Press, Cambridge, 105–149.

Berger, A. 1978: Long-term variations of caloric insolation resulting from the Earth's orbital elements. *Quaternary Research 9*, 139–167.

Bond, G., Broecker, W., Johnsen, S., McManus, J., Labeyrie, L., Jouzel, J. & Bonani, G. 1993: Correlations between climate records from North Atlantic sediments and Greenland ice. *Nature 365*, 143–147.

Broecker, W. S. 1991: The great ocean conveyor. *Oceanography 4*, 79–89.

Caralp, M. 1989: Abundance of *Bulimina exilis* and *Melonis barleeanum*: Relationship to the Quality of Marine Organic Matter. *Geo-Marine Letters 9*, 37–43.

Carstens, J., Hebbeln, D. & Wefer, G. 1997: Distribution of planktic foraminifera at the ice margin in the Arctic (Fram Strait). *Marine Micropaleontology 29*, 257–269.

Chauhan, T., Rasmussen, T. L., Noormets, R., Jakobsson, M. & Hogan, K. A. 2014: Glacial history and paleoceanography of the southern Yermak Plateau since 132 ka BP. *Quaternary Science Reviews 92*, 155–169.

Clark, P. U., Dyke, A. S., Shakun, J. D., Carlson, A. E., Clark, J., Wohlfarth, B., Mitrovica, J. X., Hostetler, S. W. & McCabe, A. M. 2009: The Last Glacial Maximum. *Science 325*, 710–714.

Corliss, B. H. 1991: Morphology and microhabitat preferences of benthic foraminifera from the northwest Atlantic Ocean. *Marine Micropaleontology 17*, 195–236.

Cottier, F., Tverberg, V., Inall, M., Svendsen, H., Nilsen, F. & Griffiths, C. 2005: Water mass modification in an Arctic fjord through cross-shelf exchange: The seasonal hydrography of Kongsfjorden, Svalbard. *Journal of Geophysical Research: Oceans (1978–2012) 110*

Darby, D. A., Bischof, J. F. & Jones, G. A. 1997: Radiocarbon chronology of depositional regimes in the western Arctic Ocean. *Deep Sea Research Part II: Topical Studies in Oceanography 44*, 1745–1757.

Darling, K. F., Kucera, M., Kroon, D. & Wade, C. M. 2006: A resolution for the coiling direction paradox in Neogloboquadrina pachyderma. *Paleoceanography 21*.

Dmitrenko, I. A., Polyakov, I. V., Kirillov, S. A., Timokhov, L. A., Simmons, H. L., Ivanov, V. V. & Walsh, D. 2006: Seasonal variability of Atlantic water on the continental slope of the Laptev Sea during 2002–2004. *Earth and Planetary Science Letters 244*, 735-743.

Dokken, T. M. & Hald, M. 1996: Rapid climatic shifts during isotope stages 2–4 in the Polar North Atlantic. *Geology 24*, 599–602.

Duplessy, J.-C., Moyes, J. & Pujol, C. 1980: Deep water formation in the North Atlantic Ocean during the last ice age. *Nature 286*, 479–482.

Duplessy, J. C., Ivanova, E., Murdmaa, I., Paterne, M. & Labeyrie, L. 2001: Holocene paleoceanography of the northern Barents Sea and variations of the northward heat transport by the Atlantic Ocean. *Boreas 30*, 2–16.

Dylmer, C., Giraudeau, J., Eynaud, F., Husum, K. & Vernal, A. D. 2013: Northward advection of Atlantic water in the eastern Nordic Seas over the last 3000 yr. *Climate of the Past 9*, 1505–1518.

Fahl, K. & Stein, R. 2012: Modern seasonal variability and deglacial/Holocene change of central Arctic Ocean sea-ice cover: New insights from biomarker proxy records. *Earth and Planetary Science Letters 351*, 123-133.

Fronval, T. & Jansen, E. 1997: Eemian and early Weichselian (140–60 ka) paleoceanography and paleoclimate in the Nordic seas with comparisons to Holocene conditions. *Paleoceanography 12*, 443–462.

Green, K. E. 1960: Ecology of some Arctic foraminifera. *Micropaleontology*, 57–78.

Haake, F.-W. & Pflaumann, U. W. E. 1989: Late Pleistocene foraminiferal stratigraphy on the Vøring Plateau, Norwegian Sea. *Boreas 18*, 343–356.

Hald, M. & Aspeli, R. 1997: Rapid climatic shifts of the northern Norwegian Sea during the last deglaciation and the Holocene. *Boreas 26*, 15–28.

Hald, M., Dokken, T. & Mikalsen, G. 2001: Abrupt climatic change during the last interglacial–glacial cycle in the polar North Atlantic. *Marine Geology 176*, 121–137.

Hald, M. & Korsun, S. 1997: Distribution of modern benthic foraminifera from fjords of Svalbard, European Arctic. *The Journal of Foraminiferal Research 27*, 101–122.

Hald, M. & Steinsund, P. 1996: Benthic foraminifera and carbonate dissolution in the surface sediments of the Barents and Kara Seas. *Surface-sediment composition and sedimentary processes in the central Arctic Ocean and along the Eurasian Continental Margin. Berichte zur Polarforschung 212*, 285–307.

Hald, M. & Steinsund, P. I. 1992: Distribution of surface sediment benthic foraminifera in the southwestern Barents Sea. *The Journal of Foraminiferal Research 22*, 347–362.

Hebbeln, D., Dokken, T., Andersen, E. S., Hald, M. & Elverhoi, A. 1994: Moisture supply for northern ice-sheet growth during the Last Glacial Maximum. *Nature 370*, 357–360.

Hebbeln, D., Henrich, R. & Baumann, K. H. 1998: Paleoceanography of the last interglacial/glacial cycle in the Polar North Atlantic. *Quaternary Science Reviews 17*, 125–153.

Hebbeln, D. & Wefer, G. 1997: Late Quaternary paleoceanography in the Fram Strait. *Paleoceanography 12*, 65–78.

Heinrich, H. 1988: Origin and consequences of cyclic ice rafting in the northeast Atlantic Ocean during the past 130,000 years. *Quaternary Research 29*, 142–152.

Heinz, P., Kitazato, H., Schmiedl, G. & Hemleben, C. 2001: Response of deep-sea benthic foraminifera from the Mediterranean Sea to simulated phytoplankton pulses under laboratory conditions. *The Journal of Foraminiferal Research 31*, 210–227.

Holland, D. M., Thomas, R. H., De Young, B., Ribergaard, M. H. & Lyberth, B. 2008: Acceleration of Jakobshavn Isbrae triggered by warm subsurface ocean waters. *Nature geoscience 1*, 659-664.

Hopkins, T. S. 1991: The GIN Sea—a synthesis of its physical oceanography and literature review 1972–1985. *Earth-Science Reviews 30*, 175-318.

Husum, K. & Hald, M. 2004: Modern foraminiferal distribution in the subarctic Malangen fjord and adjoining shelf, northern Norway. *The Journal of Foraminiferal Research 34*, 34–48.

Ivanov, V. V., Polyakov, I. V., Dmitrenko, I. A., Hansen, E., Repina, I. A., Kirillov, S. A., Mauritzen, C., Simmons, H. & Timokhov, L. A. 2009: Seasonal variability in Atlantic water off Spitsbergen. *Deep Sea Research Part I: Oceanographic Research Papers 56*, 1-14.

Jakobsson, M., Mayer, L., Coakley, B., Dowdeswell, J. A., Forbes, S., Fridman, B., Hodnesdal, H., Noormets, R., Pedersen, R., Rebesco, M., Schenke, H. W., Zarayskaya, Y., Accettella, D., Armstrong, A., Anderson, R. M., Bienhoff, P., Camerlenghi, A., Church, I., Edwards, M., Gardner, J. V., Hall, J. K., Hell, B., Hestvik, O., Kristoffersen, Y., Marcussen, C., Mohammad, R., Mosher, D., Nghiem, S. V., Pedrosa, M. T., Travaglini, P. G. & Weatherall, P. 2012: The International Bathymetric Chart of the Arctic Ocean (IBCAO) Version 3.0. *Geophysical Research Letters 39*, L12609.

Jakobsson, M., Andreassen, K., Bjarnadóttir, L. R., Dove, D., Dowdeswell, J. A., England, J. H., Funder, S., Hogan, K., Ingólfsson, Ó., Jennings, A., Krog Larsen, N., Kirchner, N., Landvik, J. Y., Mayer, L., Mikkelsen, N., Möller, P., Niessen, F., Nilsson, J., O'Regan, M., Polyak, L., Nørgaard-Pedersen, N. & Stein, R. 2014: Arctic Ocean glacial history. *Quaternary Science Reviews 92*, 40–67.

Jennings, A. E. & Helgadottir, G. 1994: Foraminiferal assemblages from the fjords and shelf of eastern Greenland. *The Journal of Foraminiferal Research 24*, 123–144.

Jennings, A. E., Weiner, N. J., Helgadottir, G. & Andrews, J. T. 2004: Modern foraminiferal faunas of the southwestern to northern Iceland shelf: oceanographic and environmental controls. *The Journal of Foraminiferal Research 34*, 180–207.

Jessen, S. P., Rasmussen, T. L., Nielsen, T. & Solheim, A. 2010: A new Late Weichselian and Holocene marine chronology for the western Svalbard slope 30,000–0 cal years BP. *Quaternary Science Reviews 29*, 1301–1312.

Jones, G. A. & Keigwin, L. D. 1988: Evidence from Fram Strait (78°N) for early deglaciation. *Nature 336*, 56–59.

794 Juggins, S. 2007: C2 Version 1.5 User guide. *Software for ecological and palaeoecological data analysis and visualisation. Newcastle University, Newcastle upon Tyne, UK 73*.

796 Knies, J., Kleiber, H.-P., Matthiessen, J., Müller, C. & Nowaczyk, N. 2001: Marine ice-rafted debris records constrain maximum extent of Saalian and Weichselian ice-sheets along the northern Eurasian margin. *Global and Planetary Change 31*, 45–64.

799 Knies, J., Nowaczyk, N., Müller, C., Vogt, C. & Stein, R. 2000: A multiproxy approach to reconstruct the environmental changes along the Eurasian continental margin over the last 150 000 years. *Marine Geology 163*, 317–344.

802 Knies, J. & Stein, R. 1998: New aspects of organic carbon deposition and its paleoceanographic implications along the northern Barents Sea margin during the last 30,000 years. *Paleoceanography 13*, 384–394.

805 Knies, J., Vogt, C. & Stein, R. 1999: Late Quaternary growth and decay of the Svalbard/Barents Sea ice sheet and paleoceanographic evolution in the adjacent Arctic Ocean. *Geo-Marine Letters 18*, 195–202.

808 Koç, N., Klitgaard-Kristensen, D., Hasle, K., Forsberg, C. F. & Solheim, A. 2002: Late glacial palaeoceanography of Hinlopen Strait, northern Svalbard. *Polar Research 21*, 307–314.

810 Korsun, S. & Hald, M. 1998: Modern Benthic Foraminifera off Novaya Zemlya Tidewater Glaciers, Russian Arctic. *Arctic and Alpine Research 30*, 61–77.

812 Korsun, S. & Hald, M. 2000: Seasonal dynamics of benthic foraminifera in a glacially fed fjord of Svalbard, European Arctic. *The Journal of Foraminiferal Research 30*, 251–271.

814 Korsun, S. & Polyak, L. 1989: Distribution of benthic foraminiferal morphogroups in the Barents Sea. *Oceanology 29*, 838–844.

816 Kristensen, D. K., Rasmussen, T. L. & Koç, N. 2013: Palaeoceanographic changes in the northern Barents Sea during the last 16 000 years – new constraints on the last deglaciation of the Svalbard–Barents Sea Ice Sheet. *Boreas 42*, 798–813.

819 Linke, P. & Lutze, G. F. 1993: Microhabitat preferences of benthic foraminifera—a static concept or a dynamic adaptation to optimize food acquisition? *Marine Micropaleontology 20*, 215–234.

821 Lloyd, J. M., Kroon, D., Boulton, G. S., Laban, C. & Fallick, A. 1996: Ice rafting history from the Spitsbergen ice cap over the last 200 kyr. *Marine Geology 131*, 103–121.

823 Lubinski, D. J., Korsun, S., Polyak, L., Forman, S. L., Lehman, S. J., Herlihy, F. A. & Miller, G. H. 1996: The last deglaciation of the Franz Victoria Trough, northern Barents Sea. *Boreas 25*, 89–100.

825 Lubinski, D. J., Polyak, L. & Forman, S. L. 2001: Freshwater and Atlantic water inflows to the deep northern Barents and Kara seas since ca 13 ^{14}C ka: foraminifera and stable isotopes. *Quaternary Science Reviews 20*, 1851–1879.

Mackensen, A. & Hald, M. 1988: *Cassidulina teretis* Tappan and *C. laevigata* d'Orbigny: Their modern and late Quaternary distribution in northern seas. *The Journal of Foraminiferal Research 18*, 16–24.

Mackensen, A., Sejrup, H. P. & Jansen, E. 1985: The distribution of living benthic foraminifera on the continental slope and rise off southwest Norway. *Marine Micropaleontology 9*, 275–306.

Mangerud, J., Bondevik, S., Gulliksen, S., Karin Hufthammer, A. & Høisæter, T. 2006: Marine 14C reservoir ages for 19th century whales and molluscs from the North Atlantic. *Quaternary Science Reviews 25*, 3228-3245

Mangerud, J. A. N., Dokken, T., Hebbeln, D., Heggen, B., IngÓLfsson, Ó., Landvik, J. Y., Mejdahl, V., Svendsen, J. I. & Vorren, T. O. 1998: Fluctuations of the Svalbard-Barents Sea Ice Sheet during the last 150 000 years. *Quaternary Science Reviews 17*, 11–42.

Marcott, S. A., Clark, P. U., Padman, L., Klinkhammer, G. P., Springer, S. R., Liu, Z., Otto-Bliesner, B. L., Carlson, A. E., Ungerer, A. & Padman, J. 2011: Ice-shelf collapse from subsurface warming as a trigger for Heinrich events. *Proceedings of the National Academy of Sciences 108*, 13415–13419.

Martinson, D. G., Pisias, N. G., Hays, J. D., Imbrie, J., Moore, T. C. & Shackleton, N. J. 1987: Age Dating and the Orbital Theory of the Ice Ages - Development of a High-Resolution 0 to 300,000-Year Chronostratigraphy. *Quaternary Research 27*, 1–29.

Mudie, P. J., Keen, C. E., Hardy, I. A. & Vilks, G. 1984: Multivariate analysis and quantitative paleoecology of benthic foraminifera in surface and Late Quaternary shelf sediments, northern Canada. *Marine Micropaleontology 8*, 283–313.

Murray, J. W. 2006: *Ecology and applications of Benthic foraminifera*. Cambridge University Press, Cambridge.

Müller, J., Massé, G., Stein, R. & Belt, S. T. 2009: Variability of sea-ice conditions in the Fram Strait over the past 30,000 years. *Nature geoscience 2*, 772–776.

Müller, J., Werner, K., Stein, R., Fahl, K., Moros, M. & Jansen, E. 2012: Holocene cooling culminates in sea ice oscillations in Fram Strait. *Quaternary Science Reviews 47*, 1–14.

März, C., Stratmann, A., Matthießen, J., Meinhardt, A.-K., Eckert, S., Schnetger, B., Vogt, C., Stein, R. & Brumsack, H.-J. 2011: Manganese-rich brown layers in Arctic Ocean sediments: composition, formation mechanisms, and diagenetic overprint. *Geochimica et Cosmochimica Acta 75*, 7668–7687.

Nørgaard-Pedersen, N. 1997: Late Quaternary Arctic Ocean sediment records: surface ocean conditions and provenance of ice-rafted debris. *GEOMAR*. Research Centre for Marine Geosciences, Kiel, Germany.

Nørgaard-Pedersen, N., Spielhagen, R. F., Erlenkeuser, H., Grootes, P. M., Heinemeier, J. & Knies, J. 2003: Arctic Ocean during the Last Glacial Maximum: Atlantic and polar domains of surface water mass distribution and ice cover. *Paleoceanography 18*, 1063.

Onarheim, I. H., Smedsrud, L. H., Ingvaldsen, R. B. & Nilsen, F. 2014: Loss of sea ice during winter north of Svalbard. *Tellus A 66*.

Pados, T. & Spielhagen, R. F. 2014: Species distribution and depth habitat of recent planktic foraminifera in Fram Strait, Arctic Ocean. *Polar Research 33*, 22483.

Polyak, L., Best, K. M., Crawford, K. A., Council, E. A. & St-Onge, G. 2013: Quaternary history of sea ice in the western Arctic Ocean based on foraminifera. *Quaternary Science Reviews 79*, 145–156.

Polyak, L., Korsun, S., Febo, L. A., Stanovoy, V., Khusid, T., Hald, M., Paulsen, B. E. & Lubinski, D. J. 2002: Benthic foraminiferal assemblages from the southern Kara Sea, a river-influenced Arctic marine environment. *The Journal of Foraminiferal Research 32*, 252–273.

Polyak, L. & Mikhailov, V. 1996: Post-glacial environments of the southeastern Barents Sea: foraminiferal evidence. *Geological Society, London, Special Publications 111*, 323–337.

Polyak, L. & Solheim, A. 1994: Late-and postglacial environments in the northern Barents Sea west of Franz Josef Land. *Polar Research 13*, 197–207.

Poole, D. A. R., Dokken, T. M., Hald, M. & Polyak, L. 1994: Stable isotope fractionation in recent benthic foraminifera from the Barents and Kara Seas. *Poole, D. A. R, Neogene and Quaternary Paleoenvironments on the North Norwegian Shelf. Ph. D. Thesis, Department of Geology, University of Tromsø, Norway,* 1–82.

Rasmussen, T. L. 2005: Systematic paleontology and ecology of benthic foraminifera from the Plio-Pleistocene Kallithea Bay section, Rhodes, Greece. *Cushman Foundation Special Publication 39*, 53–157.

Rasmussen, T. L., Balbon, E., Thomsen, E., Labeyrie, L. & Van Weering, T. C. E. 1999: Climate records and changes in deep outflow from the Norwegian Sea~ 150–55 ka. *Terra Nova 11*, 61–66.

Rasmussen, T. L. & Thomsen, E. 2004: The role of the North Atlantic Drift in the millennial timescale glacial climate fluctuations. *Palaeogeography, Palaeoclimatology, Palaeoecology 210*, 101–116.

Rasmussen, T. L. & Thomsen, E. 2005: Foraminifera and paleoenvironment of the Plio-Pleistocene Kallithea Bay section, Rhodes, Greece: Evidence for cyclic sedimentation and shallow-water sapropels. *Cushman Foundation for Foraminiferal Research, Special Publication 39*, 15–51.

Rasmussen, T. L., Thomsen, E. & Nielsen, T. 2014a: Water mass exchange between the Nordic seas and the Arctic Ocean on millennial timescale during MIS 4–MIS 2. *Geochemistry, Geophysics, Geosystems 15*, 530–544.

895 Rasmussen, T. L., Thomsen, E., Labeyrie, L. & van Weering, T. C. E. 1996a: Circulation changes in the Faeroe-Shetland Channel correlating with cold events during the last glacial period (58–10 ka). *Geology 24*, 937–940.

898 Rasmussen, T. L., Thomsen, E., Skirbekk, K., Ślubowska-Woldengen, M., Klitgaard Kristensen, D. & Koç, N. 2014b: Spatial and temporal distribution of Holocene temperature maxima in the northern Nordic seas: interplay of Atlantic-, Arctic-and polar water masses. *Quaternary Science Reviews 92*, 280-291

902 Rasmussen, T. L., Thomsen, E., Ślubowska, M. A., Jessen, S., Solheim, A. & Koç, N. 2007: Paleoceanographic evolution of the SW Svalbard margin (76°N) since 20,000 14C yr BP. *Quaternary Research 67*, 100–114.

905 Rasmussen, T. L., Thomsen, E., Van Weering, T. C. E. & Labeyrie, L. 1996b: Rapid changes in surface and deep water conditions at the Faeroe Margin during the last 58,000 years. *Paleoceanography 11*, 757–771.

908 Reimer, P. J., Bard, E., Bayliss, A., Beck, J. W., Blackwell, P. G., Ramsey, C. B., Buck, C. E., Cheng, H., Edwards, R. L., Friedrich, M., Grootes, P. M., Guilderson, T. P., Haflidason, H., Hajdas, I., C, H., Heaton, T. J., Hoffmann, D. L., Hogg, A. G., Hughen, K. A., Kaiser, K. F., Kromer, B., Manning, S. W., M, N., Reimer, R. W., Richards, D. A., Scott, D. B., Southon, J. R., Staff, R. A., Turney, C. S. M. & Plicht, J. v. d. 2013: IntCal13 and Marine13 radiocarbon age calibration curves 0–50,000 years cal BP. *Radiocarbon 55*, 1869–1887.

914 Risebrobakken, B., Dokken, T., Smedsrud, L. H., Andersson, C., Jansen, E., Moros, M. & Ivanova, E. V. 2011: Early Holocene temperature variability in the Nordic Seas: The role of oceanic heat advection versus changes in orbital forcing. *Paleoceanography 26*, PA4206.

917 Risebrobakken, B., Moros, M., Ivanova, E. V., Chistyakova, N. & Rosenberg, R. 2010: Climate and oceanographic variability in the SW Barents Sea during the Holocene. *The Holocene*, 1–13.

919 Rudels, B., Anderson, L. G., Eriksson, P., Fahrbach, E., Jakobsson, M., Jones, P., Melling, H., Prinsenberg, S., Shauer, U. & Yao, T. 2011: *Observations in the Ocean*. Springer, Berlin.

921 Rytter, F., Knudsen, K. L., Seidenkrantz, M. S. & Eiríksson, J. 2002: Modern distribution of benthic foraminifera on the North Icelandic shelf and slope. *The Journal of Foraminiferal Research 32*, 217–244.

924 Saher, M., Kristensen, D. K., Hald, M., Korsun, S. & Jørgensen, L. L. 2009: Benthic foraminifera assemblages in the Central Barents Sea: an evaluation of the effect of combining live and total fauna studies in tracking environmental change. *Norwegian Journal of Geology 89*, 149–161.

927 Sarnthein, M., Jansen, E., Weinelt, M., Arnold, M., Duplessy, J. C., Erlenkeuser, H., Flatøy, A., Johannessen, G., Johannessen, T., Jung, S., Koc, N., Labeyrie, L., Maslin, M., Pflaumann, U. &

Schulz, H. 1995: Variations in Atlantic surface ocean paleoceanography, 50°-80°N: A time-slice record of the last 30,000 years. *Paleoceanography 10*, 1063–1094.

Sarnthein, M., Van Kreveld, S., Erlenkeuser, H., Grootes, P. M., Kucera, M., Pflaumann, U. & Schulz, M. 2003: Centennial-to-millennial-scale periodicities of Holocene climate and sediment injections off the western Barents shelf, 75°N. *Boreas 32*, 447–461.

Seidenkrantz, M.-S. 1995: *Cassidulina teretis* Tappan and *Cassidulina neoteretis* new species (Foraminifera): stratigraphic markers for deep sea and outer shelf areas. *Journal of Micropalaeontology 14*, 145–157.

Seidenkrantz, M.-S. 2013: Benthic foraminifera as palaeo sea-ice indicators in the subarctic realm–examples from the Labrador Sea–Baffin Bay region. *Quaternary Science Reviews 79*, 135–144.

Sejrup, H., Birks, H., Klitgaard Kristensen, D. & Madsen, H. 2004: Benthonic foraminiferal distributions and quantitative transfer functions for the northwest European continental margin. *Marine Micropaleontology 53*, 197–226.

Sejrup, H. P., Fjaeran, T., Hald, M., Beck, L., Hagen, J., Miljeteig, I., Morvik, I. & Norvik, O. 1981: Benthonic foraminifera in surface samples from the Norwegian continental margin between 62°N and 65°N. *The Journal of Foraminiferal Research 11*, 277–295.

Simstich, J., Sarnthein, M. & Erlenkeuser, H. 2003: Paired δ^{18}O signals of *Neogloboquadrina pachyderma* (s) and *Turborotalita quinqueloba* show thermal stratification structure in Nordic Seas. *Marine Micropaleontology 48*, 107–125.

Ślubowska-Woldengen, M., Koc, N., Rasmussen, T. L., Klitgaard-Kristensen, D., Hald, M. & Jennings, A. E. 2008: Time-slice reconstructions of ocean circulation changes on the continental shelf in the Nordic and Barents Seas during the last 16,000 cal yr BP. *Quaternary Science Reviews 27*, 1476–1492.

Ślubowska-Woldengen, M., Rasmussen, T. L., Koç, N., Klitgaard-Kristensen, D., Nilsen, F. & Solheim, A. 2007: Advection of Atlantic Water to the western and northern Svalbard shelf since 17,500 cal yr BP. *Quaternary Science Reviews 26*, 463–478.

Ślubowska, M. A., Koç, N., Rasmussen, T. L. & Klitgaard-Kristensen, D. 2005: Changes in the flow of Atlantic water into the Arctic Ocean since the last deglaciation: evidence from the northern Svalbard continental margin, 80°N. *Paleoceanography 20*, PA4014.

Solomon, S. 2007: *Climate change 2007-the physical science basis: Working group I contribution to the fourth assessment report of the IPCC*. Cambridge University Press, Cambridge.

Spielhagen, R. F., Baumann, K.-H., Erlenkeuser, H., Nowaczyk, N. R., Nørgaard-Pedersen, N., Vogt, C. & Weiel, D. 2004: Arctic Ocean deep-sea record of northern Eurasian ice sheet history. *Quaternary Science Reviews 23*, 1455–1483.

Spielhagen, R. F., Erlenkeuser, H. & Siegert, C. 2005: History of freshwater runoff across the Laptev Sea (Arctic) during the last deglaciation. *Global and Planetary Change 48*, 187-207.

Stanford, J., Rohling, E., Bacon, S., Roberts, A., Grousset, F. & Bolshaw, M. 2011: A new concept for the paleoceanographic evolution of Heinrich event 1 in the North Atlantic. *Quaternary Science Reviews 30*, 1047–1066.

Stein, R., Schubert, C., Vogt, C. & Fütterer, D. 1994: Stable isotope stratigraphy, sedimentation rates, and salinity changes in the Latest Pleistocene to Holocene eastern central Arctic Ocean. *Marine Geology 119*, 333–355.

Steinsund, P. I. 1994: Benthic foraminifera in surface sediments of the Barents and Kara seas: Modern and late Quaternary applications. *PhD Thesis, University of Tromsø, Tromsø, Norway.*

Steinsund, P. I. & Hald, M. 1994: Recent calcium carbonate dissolution in the Barents Sea: Paleoceanographic applications. *Marine Geology 117*, 303–316.

Stuiver, M. & Reimer, J. 1993: Extended 14C data base and revised CALIB 3.014 C age calibration program. *Editorial Comment 35*, 215–230.

Svendsen, H., Beszczynska-Møller, A., Hagen, J. O., Lefauconnier, B., Tverberg, V., Gerland, S., Ørbøk, J. B., Bischof, K., Papucci, C. & Zajaczkowski, M. 2002: The physical environment of Kongsfjorden–Krossfjorden, an Arctic fjord system in Svalbard. *Polar Research 21*, 133-166.

Svendsen, J. I. & Mangerud, J. 1997: Holocene glacial and climatic variations on Spitsbergen, Svalbard. *The Holocene 7*, 45–57.

Svensson, A., Andersen, K. K., Bigler, M., Clausen, H. B., Dahl-Jensen, D., Davies, S., Johnsen, S. J., Muscheler, R., Parrenin, F. & Rasmussen, S. O. 2008: A 60 000 year Greenland stratigraphic ice core chronology. *Climate of the Past 4*, 47–57.

Thomas, E., Booth, L., Maslin, M. & Shackleton, N. 1995: Northeastern Atlantic benthic foraminifera during the last 45,000 years: changes in productivity seen from the bottom up. *Paleoceanography 10*, 545–562.

Vogt, C., Knies, J., Spielhagen, R. F. & Stein, R. 2001: Detailed mineralogical evidence for two nearly identical glacial/deglacial cycles and Atlantic water advection to the Arctic Ocean during the last 90,000 years. *Global and Planetary Change 31*, 23–44.

Volkmann, R. 2000: Planktic foraminifers in the outer Laptev Sea and the Fram Strait—modern distribution and ecology. *The Journal of Foraminiferal Research 30*, 157–176.

Werner, K., Spielhagen, R. F., Bauch, D., Hass, H. C. & Kandiano, E. 2013: Atlantic Water advection versus sea-ice advances in the eastern Fram Strait during the last 9 ka: Multiproxy evidence for a two-phase Holocene. *Paleoceanography 28*, 283–295.

Wollenburg, J. E., Knies, J. & Mackensen, A. 2004: High-resolution paleoproductivity fluctuations during the past 24 kyr as indicated by benthic foraminifera in the marginal Arctic Ocean. *Palaeogeography, Palaeoclimatology, Palaeoecology 204*, 209–238.

Wollenburg, J. E. & Kuhnt, W. 2000: The response of benthic foraminifers to carbon flux and primary production in the Arctic Ocean. *Marine Micropaleontology 40*, 189-231.

Wollenburg, J. E., Kuhnt, W. & Mackensen, A. 2001: Changes in Arctic Ocean paleoproductivity and hydrography during the last 145 kyr: The benthic foraminiferal record. *Paleoceanography 16*, 65–77.

Wollenburg, J. E. & Mackensen, A. 1998: Living benthic foraminifers from the central Arctic Ocean: faunal composition, standing stock and diversity. *Marine Micropaleontology 34*, 153–185.

Wollenburg, J. E., Mackensen, A. & Kuhnt, W. 2007: Benthic foraminiferal biodiversity response to a changing Arctic palaeoclimate in the last 24,000 years. *Palaeogeography, Palaeoclimatology, Palaeoecology 255*, 195–222.

Zamelczyk, K., Rasmussen, T. L., Husum, K., Haflidason, H., de Vernal, A., Ravna, E. K., Hald, M. & Hillaire-Marcel, C. 2012: Paleoceanographic changes and calcium carbonate dissolution in the central Fram Strait during the last 20 ka. *Quaternary Research 78*, 405–416.

Core name	Lab Code	Material used	Depth (cm)	AMS ^{14}C age	Reservoir correction	Calendar year BP	AMS δ^{13}C‰
HH11-09GC#	Ua-46352	Bivalve	**Surface (0)**	103.3 ± 0.4 pMC	-	-	-0.2
	LuS 10822	Mixed planktic foraminifera	31	2010 ± 45	405 yr	1573 ± 59	N.d
	LuS 10823	Mixed planktic foraminifera	57	3770 ± 65	405 yr	3715 ± 89	N.d
	LuS 10824	Mixed benthic foraminifera	75	10610 ± 70	405 yr	11915 ± 145	N.d
	LuS 10825	Mixed benthic foraminifera	165	13270 ± 70	405 yr	15347 ± 133	N.d
	Ua-46353	Bivalve	220	14382 ± 488	405 yr	16926 ± 658	11.7
	LuS 10826	*N. pachyderma* s	240	18565 ± 85	405 yr	22011 ± 136	N.d
	Ua-46428	Bivalve	**255**	28804 ± 483	405 yr	**32310 ± 649**	6.0
	LuS 10827	*N. pachyderma* s	260	18545 ± 85	405 yr	22000 ± 125	N.d
	LuS 10828	Mixed benthic foraminifera	286	25800 ± 300	405 yr	29452 ± 405	N.d
	LuS 10829	*C. lobatulus*	**307.5**	30750 ± 400	405 yr	**34029 ± 386**	N.d
	LuS 10830	*N. pachyderma* s	335	28350 ± 500	405 yr	31854 ± 565	N.d
	LuS 10831	Mixed planktic foraminifera	380	> 42000	-	-	N.d
	Ua-46430	Bivalve	**406**	9368 ± 52	405 yr	**10067 ± 172**	0.6
	LuS 10832	*N. labradorica*	411	> 38000	-	-	N.d
JM10-02GC*	LuS 10943	Mixed benthic foraminifera	20	5350 ± 120	440 ± 52 yr	5646 ± 184 ¤	N.d
	LuS 10944	Mixed benthic foraminifera	**31**	13410±475	440 ± 52 yr	**15082 ± 542** ¤	N.d
	LuS 10945	Mixed benthic foraminifera	40	13230±450	440 ± 52 yr	14848 ± 649 ¤	N.d
	Ua-41639	Mixed planktic foraminifera	50	12941 ± 91	440 ± 52 yr	14470 ± 260	-2.8
	UBA-20117	*N. pachyderma* s	65	15054 ± 62	440 ± 52 yr	17347 ± 255	-2.4
	UBA-20540	*N. pachyderma* s	115	18514 ± 95	440 ± 52 yr	21481 ± 244	0.0
	UBA-20119	*N. pachyderma* s	120	18891 ± 77	440 ± 52 yr	22058 ± 174	-1.8
	UBA-20539	*N. pachyderma* s	157	21817±111	440 ± 52 yr	25646 ± 241	0.0
	UBA-20118	*N. pachyderma* s	160	23353±123	440 ± 52 yr	27509 ± 241	-0.1
	UBA-20120	*N. pachyderma* s	225	46567±2091	-	-	0.6
	UBA-20121	*N. pachyderma* s	270	>48874	-	-	0.5

Radiocarbon ages are calibrated using Calib 7.02 and Marine 13 software integrated with standard reservoir correction of 405 years (see text); *Radiocarbon ages are calibrated using Fairbanks calibration curve and reservoir correction suggested by Mangerud *et al.* (2006) is applied (Chauhan *et al.* 2014); ¤ New ages from core JM10-02GC, remaining ages from this core are published in Chauhan *et al.* (2014); LuS –Lund Radiocarbon Dating Laboratory, Lund, Sweden; Ua –Ångstrom Radiocarbon Laboratory, Uppsala, Sweden; UBA –^{14}CHRONO Centre for Climate, Environment and Chronology, Belfast, UK; Ages in **bold** are age reversals and not used in the age model; N.d- Not determined

Foraminifera Species and Taxonomy	Ecological preferences	References
Neogloboquadrina pachyderma (sinistral) (Ehrenberg, 1861)	Polar species. Related to Arctic and Polar Water at the surface.	Carstens *et al.* (1997); Simstich *et al.* (2003)
Turborotalita quinqueloba (Natland, 1938)	Sub-polar species. Associated with Arctic Waters and Arctic/Polar Fronts.	Bé & Tolderlund 1971; Volkmann 2000; Simstich *et al.* (2003); Pados & Spielhagen 2014
Cassidulina neoteretis Seidenkrantz, 1995	Infaunal species that prefers fine-grained, terrigenous mud. Abundant in glaciomarine environments with stable salinity and temperature. Confined to areas influenced by often cool AW with/without Polar Water or sea-ice at the surface.	Green (1960); Mackensen & Hald (1988); Jennings & Helgadottir (1994); Seidenkrantz (1995); Polyak & Mikhailov (1996); Hald & Korsun (1997); Lubinski *et al.* (2001); Rytter *et al.* (2002); Husum & Hald (2004); Jennings *et al.* (2004); Wollenburg *et al.* (2004)
Melonis barleeanus (Williamson, 1858)	Infaunal Arctic-Boreal species. Related to chilled AW, high salinities, open water to seasonal sea-ice cover and fine sediments. High sedimentation rates and steady supply of food through partially degraded organic matter.	Caralp (1989); Korsun & Polyak (1989); Linke & Lutze (1993); Steinsund (1994); Hald & Steinsund (1996); Heinz *et al.* (2001); Polyak *et al.* (2002); Jennings *et al.* (2004)
Cibicides lobatulus (Walker and Jacob, 1798)	Epifaunal species found in coarser sediments. Often attached to hard substrates. Shows good correlation with high energy environments.	Mackensen *et al.* (1985); Hald & Steinsund (1992); Hald & Korsun (1997); Murray (2006)
Astrononion gallowayi Loeblich and Tappan, 1953	Occurs in areas of coarse sediment. Indicator of enhanced bottom current activity.	Sejrup *et al.* (1981); Mackensen *et al.* (1985); Korsun & Polyak (1989); Polyak & Solheim (1994); Wollenburg & Mackensen (1998); Polyak *et al.* (2002); Jennings *et al.* (2004); Murray (2006)
Cassidulina reniforme Nørvang, 1945	Arctic species. Associated with cold AW in faunas of relatively high diversity. Also found in proximal glaciomarine environments in faunas of low diversity.	Sejrup *et al.* (1981); Mackensen *et al.* (1985); Hald & Korsun (1997); Korsun & Hald (2000)
Islandiella norcrossi (Cushman, 1933)	Arctic-Polar species. Prefers relatively high and stable bottom water salinities. Indicator of high organic content of the sediment, increased productivity and presence of the sea-ice edge and seasonal sea-ice.	Steinsund (1994); Korsun & Hald (1998); Polyak *et al.* (2002); Murray (2006); Slubowska-Woldengen *et al.* (2008)
Buccella spp.	Prefers low temperatures and use algal blooms at the sea-ice margin as food source. They indicate cold conditions with seasonal sea-ice.	Mudie *et al.* (1984); Polyak & Solheim (1994); Steinsund (1994)

Elphidium excavatum (Terquem, 1875)	Arctic-Polar species. Abundant in polar conditions and in cold bottom water. Highly adaptable to changes in food availability and thus tolerates variable environmental conditions with low salinity and low temperatures and high turbidity. Dominant in front of glaciers and in ice marginal conditions.	Linke & Lutze (1993); Steinsund (1994); Hald & Korsun (1997); Korsun & Hald (2000); Polyak *et al.* (2002); Sejrup *et al.* 2004
Nonionellina labradorica (Dawson, 1860)	Arctic-Polar species. Prefers cold water (<2 °C) of normal salinity >34.5‰ and is abundant in areas with high organic matter and high, seasonal productivity in ice marginal zones or oceanic fronts.	Mudie *et al.* (1984); Corliss (1991); Steinsund (1994); Hald & Korsun (1997); Korsun & Hald (1998); Korsun & Hald (2000); Polyak *et al.* (2002); Sejrup *et al.* (2004); Murray (2006)
Pullenia bulloides (d'Orbigny, 1826)	Infaunal species associated with high organic flux and influence of AW especially in terms of bottom water temperature. Prefers a narrow salinity interval close to 35‰ and temperature between 2 °C and 4 °C.	Haake & Pflaumann (1989); Fronval & Jansen (1997); Rasmussen *et al.* (1999); Rytter *et al.* (2002); Risebrobakken *et al.* (2010)
'Atlantic species' *Anomalinoides minimus* (Forster, 1892); *Cibicides pachyderma* (Rzehak, 1886); *Cornuloculina inconstans* Brady,1884; *Eggerella bradyi* (Cushman, 1911); *Eilohedra nipponica* Kuwano, 1962; *Gyroidina umbonata* (Silvestri, 1898); *Pyrgo* sp.; *Marginulinopsis costata* (Batsch, 1791); *Pullenia subcarinata* (d'Orbigny, 1839); *Pyrgo williamsoni* (Silvestri, 1923); *Pyrgoella irregularis* (d'Orbigny, 1839); *Robertinoides* sp.; *Sagrina subspinescens* (Cushman, 1936); *Sphaeroidina bulloides* d'Orbigny, 1826; *Triloculina oblonga* (Montagu, 1803) and *Valvulineria arctica* Green, 1959	The group has southern affinity and lives in warmer AW. They are adapted to low productivity. Meltwater and sea-ice cover during Heinrich events prevented heat loss and caused bottom water warming providing favourable conditions for this group of species.	Thomas *et al.* (1995); Rasmussen *et al.* 1996a, b); Wollenburg & Mackensen (1998); Rasmussen (2005); Rasmussen & Thomsen (2005); Rasmussen *et al.* (2007); Wollenburg *et al.* (2001, 2004, 2007)

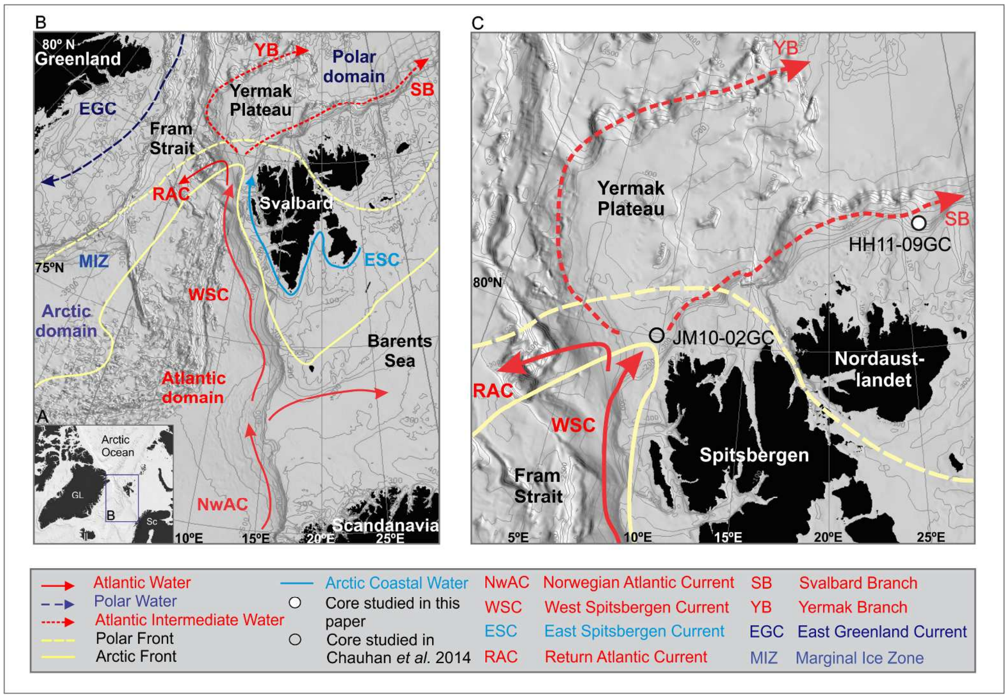

Fig. 1. A) Overview map of the Nordic Seas and the Arctic Ocean showing the location of Svalbard. B) Map of the northern Nordic Seas and the Barents Sea showing the main water masses, surface currents and oceanic fronts. C) Locations of the cores HH11-09GC (white circle) studied in this paper and the previously published sediment core JM10-02GC (open circle, Chauhan *et al.* 2014) on the northern Svalbard margin. Bathymetric map is from the International Bathymetric Chart of the Arctic Ocean (IBCAO) v3 (Jakobsson *et al.* 2012).
242x167mm (300 x 300 DPI)

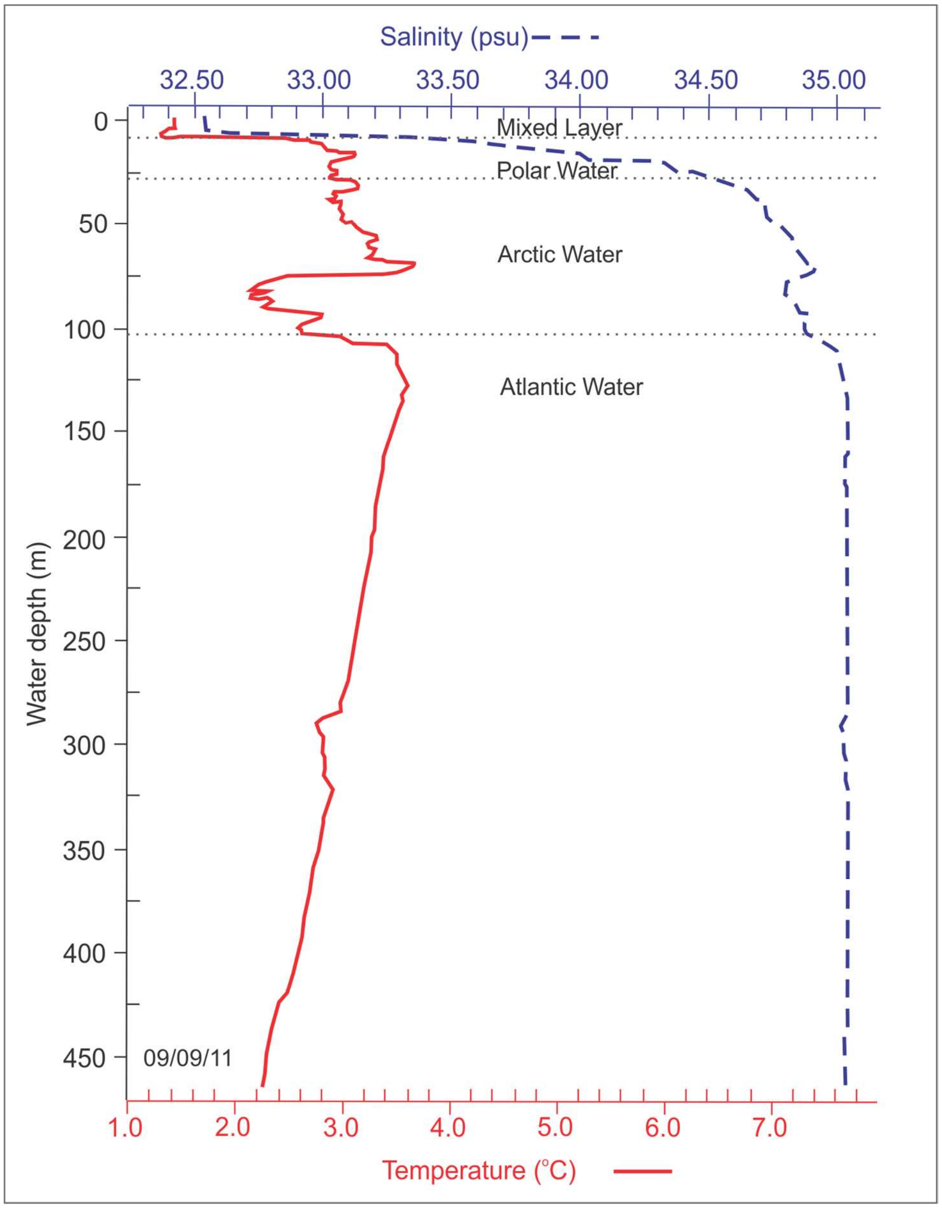

Fig. 2. CTD (Conductivity, Temperature, Depth) profile from core site HH11-09GC taken on 9th September, 2011. Different water masses are labelled.
126x162mm (300 x 300 DPI)

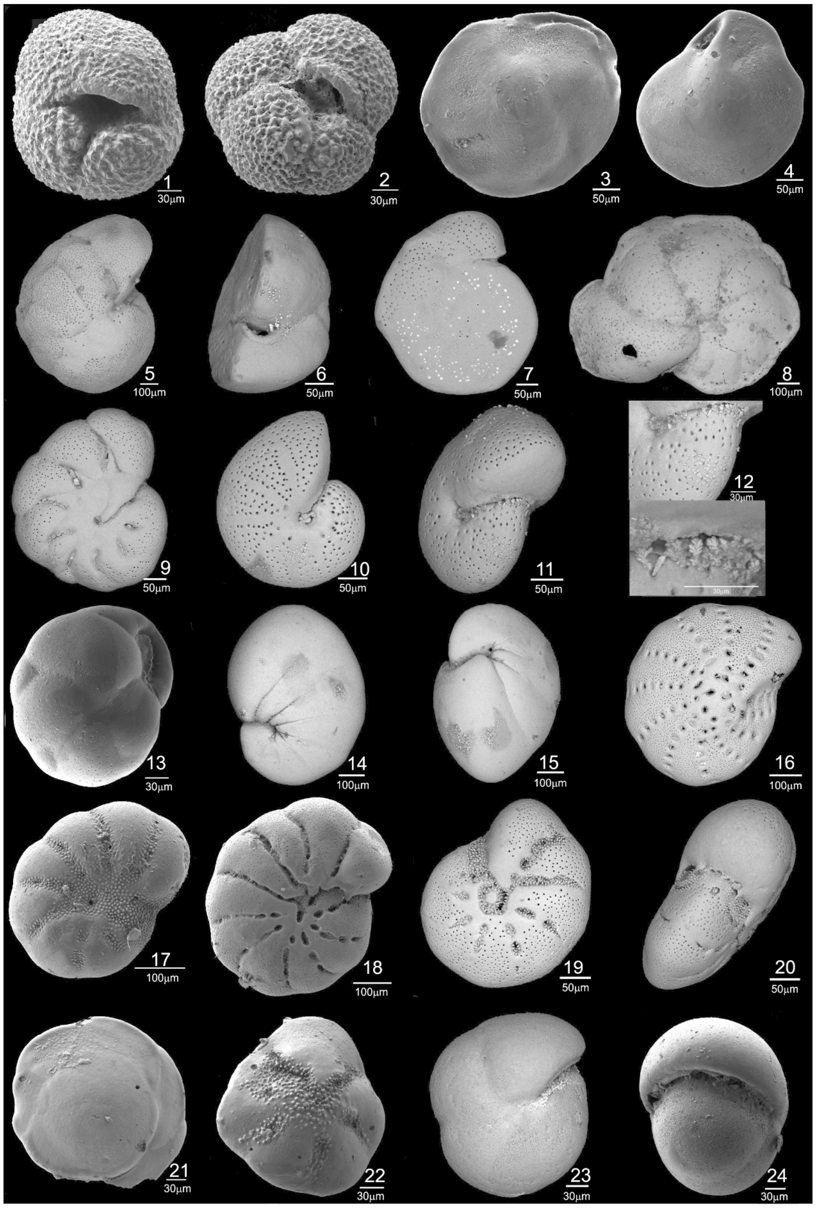

Fig. 3A. Scanning electron microscope (SEM) images of pristine benthic foraminifera used for radiocarbon dating and isotope studies: 1, 2. *Neogloboquadrina pachyderma* (sinistral); 3. *Cassidulina neoteretis*; 4. *Islandiella norcrossi*; 5, 6, 7, 8. *Cibicides lobatulus*; 9. *Astrononion gallowayi*; 10, 11, 12. *Melonis barleeanus*; 13. *Cassidulina reniforme*; 14, 15. *Nonionellina labradorica*; 16. *Elphidium tumidum*; 17. *Elphidium subarcticum*; 18, 19, 20. *Elphidium excavatum*; 21, 22. *Buccella* spp.; 23, 24. *Pullenia bulloides*. 186x276mm (300 x 300 DPI)

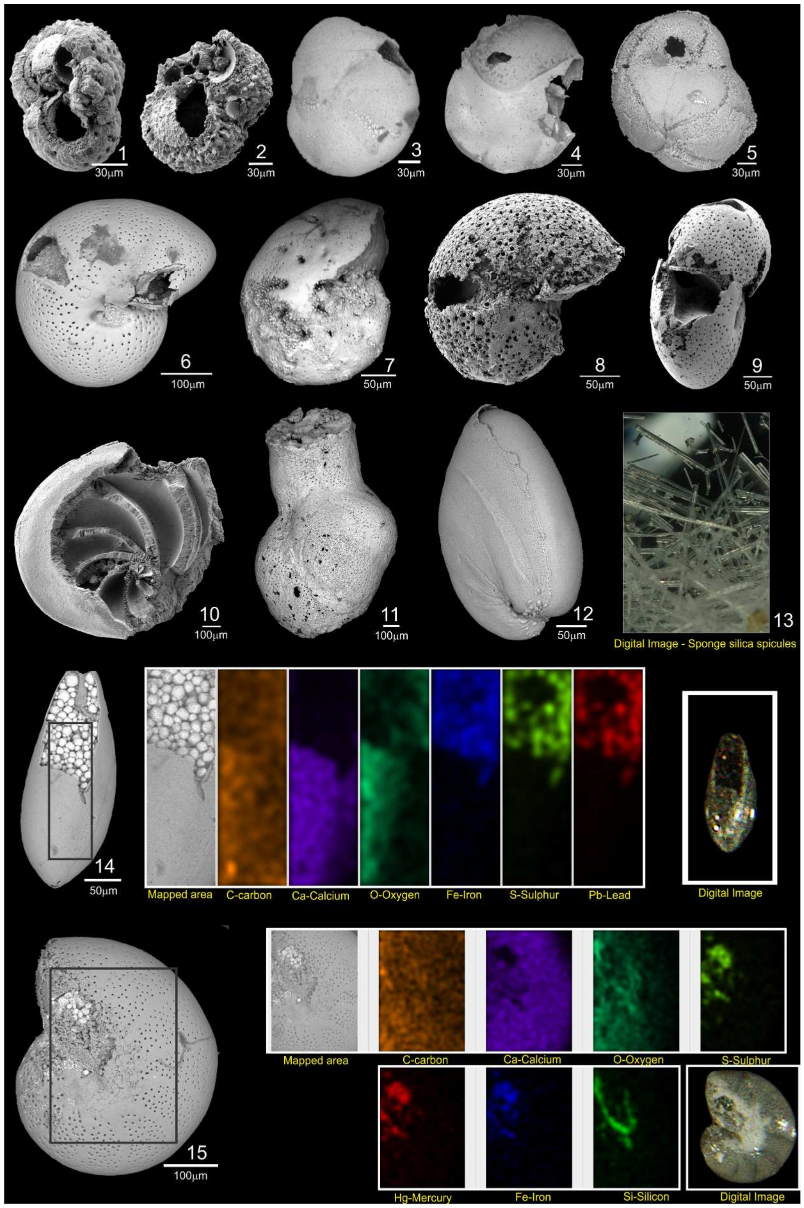

Fig. 3B. Scanning electron microscope (SEM) images of dissolved (1–12) and pyritised foraminifera (14, 15). Number 13 shows digital image of silica spicules obtained from 7–8 cm and 50–60 cm core depth of core HH11-09GC. Number 14 and 15 show SEM images, elemental composition of mapped grey square area by Energy Dispersive X-ray Spectrometry (EDS) and digital image of two pyritised specimens. 1, 2. *Neogloboquadrina pachyderma* (sinistral); 3. *Cassidulina reniforme*; 4. *Cassidulina neoteretis*; 5. *Islandiella islandica*; 6, 7, 8, 9. *Melonis barleeanus*; 10. *Cibicides lobatulus*; 11. *Rupertina stabilis*; 12. *Nonionella turgida*; 13. Silica spicules; 14. *Parafissurina* sp.; 15, *Melonis barleeanus*.
179x269mm (300 x 300 DPI)

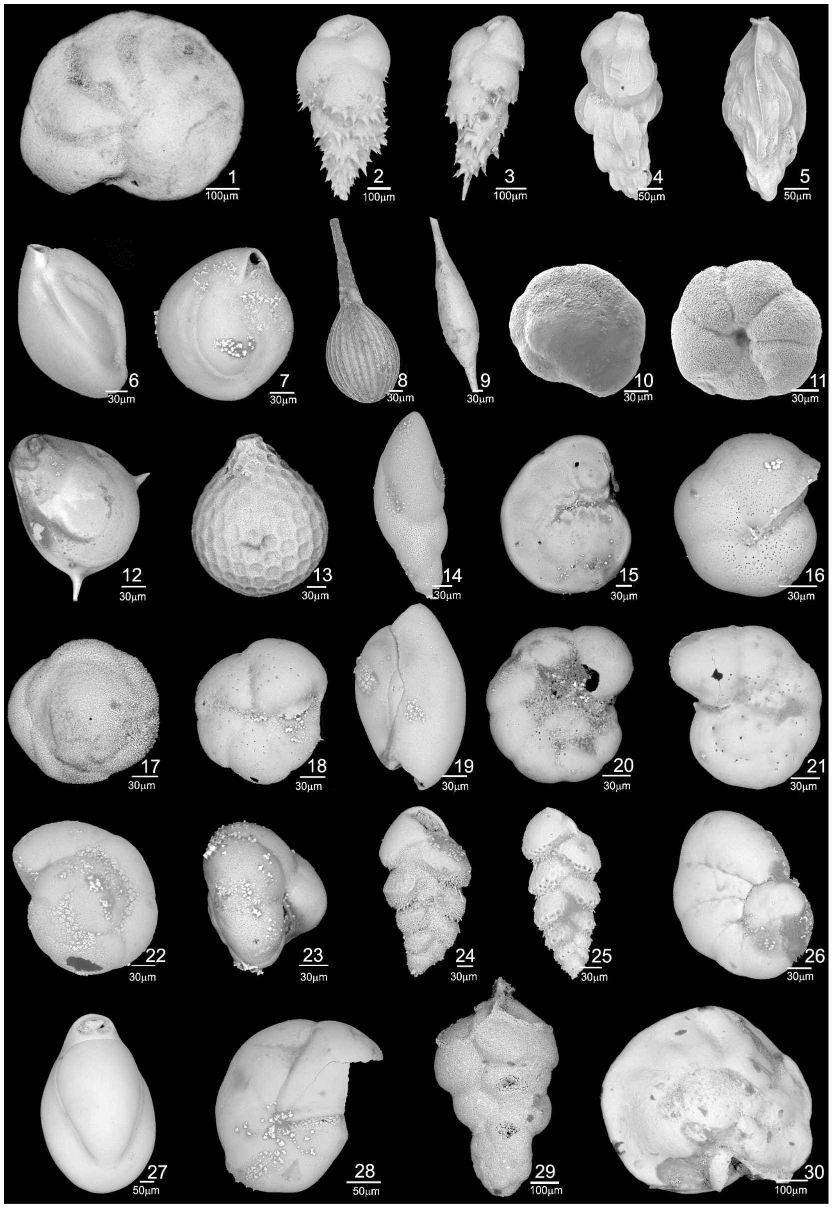

Fig. 3C. Scanning electron microscope (SEM) images of other benthic species present in core HH11-09GC (1–16) and benthic foraminifera from the 'Atlantic species group' (17–30) identified from core HH11-09GC and JM10-02GC: 1. *Cibicides wuellerstorfi*; 2. *Bulimina marginata*; 3. *Bulimina aculeata*; 4. *Trifarina fluens*; 5. *Trifarina angulosa*; 6. *Triloculina trihedra*; 7. *Millionella subrotunda*; 8. *Lagena striata*; 9. *Lagena gracillima*; 10, 11. *Ioanella tumidula*; 12. *Lenticulina* sp.; 13. *Oolina hexagona*; 14. *Stainforthia loeblichi*; 15. *Hyalinea baltica*; 16. *Pullenia osloensis*; 17, 18. *Eilohedra nipponica*; 19. *Triloculina oblonga*; 20, 21. *Anomalinoides minimus*; 22, 23. *Gyroidina umbonata*; 24, 25. *Sagrina subspinescens*; 26. *Valvulineria arctica*; 27. *Pyrgo williamsoni*; 28. *Pullenia subcarinata*; 29. *Eggerella bradyi*; 30. *Cibicides pachyderma*.
191x277mm (300 x 300 DPI)

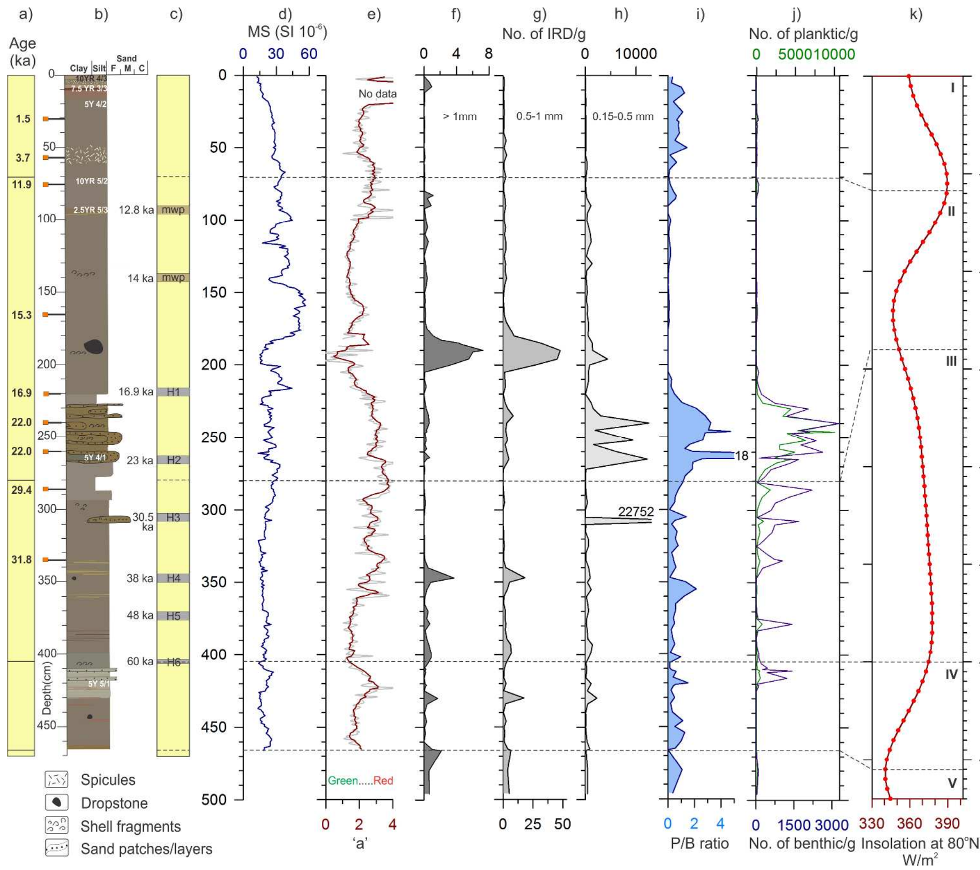

Fig. 4. Logs of the core HH11-09GC: a) Calibrated ^{14}C ages in ka; b) Lithological log; c) Boundaries and ages of Heinrich events (H1–H6) and meltwater pulse (mwp); d) Magnetic susceptibility; e) Green-red (‘a’) spectrum; f), g) and h) Concentration of IRD per gram dry weight sediment in three different size fractions (>1 mm, 0.5–1 mm and 0.15–0.5 mm, respectively); i) Planktic/benthic (P/B) ratio; j) Concentration of planktic (green) and benthic foraminifera (purple) in number per gram dry weight sediment; k) Insolation curve at 80°N (Berger 1978). Marine Isotope Stages (MIS) indicated by Roman numbers are defined based on Martinson *et al.* (1987).
324x278mm (300 x 300 DPI)

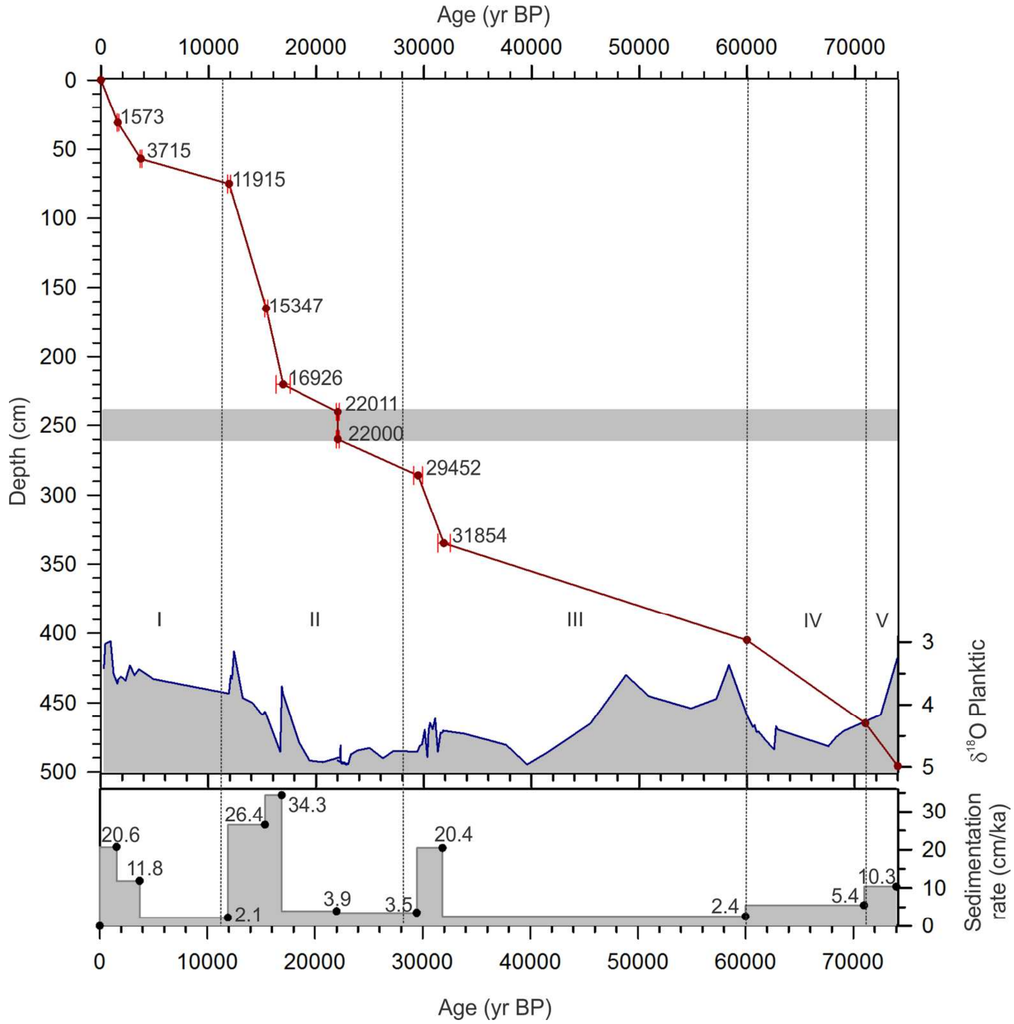

Fig. 5. Age-depth plot, planktic $\delta^{18}O$ record and sedimentation rates for core HH11-09GC. Calibrated ages in years before present (yr BP) are shown with 1 sigma error bars. Numbers in the lower panel indicate sedimentation rate in cm/ka. Grey horizontal bar in the age-depth plot marks level with identical dates (no sedimentation rate calculated). Vertical dotted lines mark Marine Isotope Stages (MIS) 1–5, which are labelled with Roman numbers.

161x163mm (300 x 300 DPI)

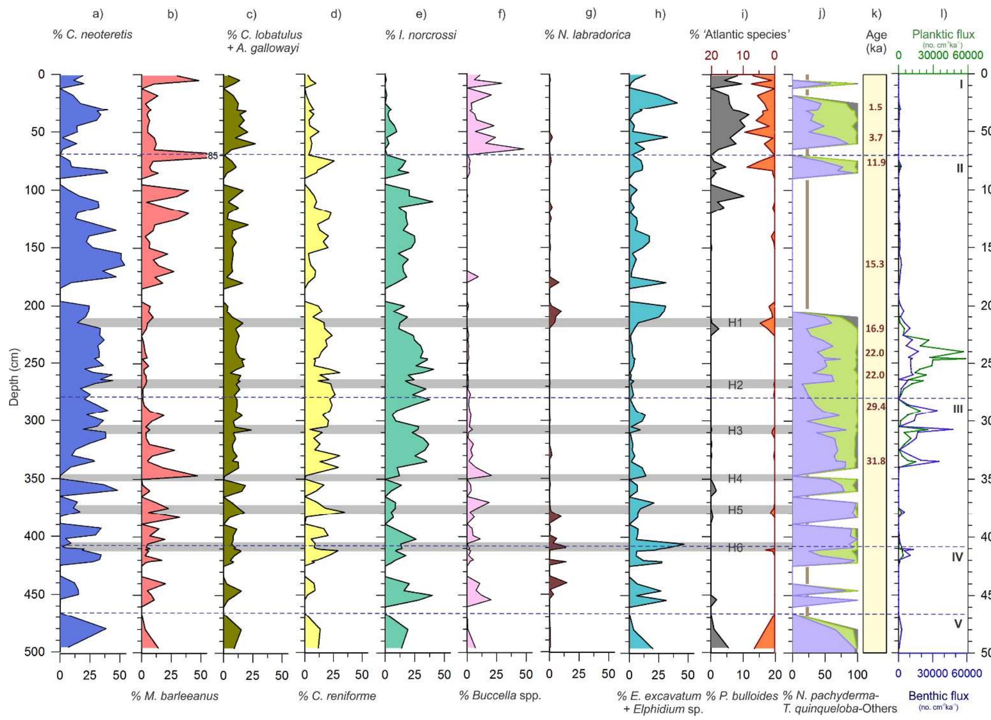

Fig. 6. a) to i) Relative abundance of most common benthic foraminiferal species. Panel i) also presents 'Atlantic species group' (see text for explanation); j) Relative abundance of planktic foraminiferal species: *N. pachyderma* (sinistral) (violet), *T. quinqueloba* (green) and other planktic species (grey). Vertical bars mark barren intervals; k) Calibrated ^{14}C ages in ka; l) Accumulation rates (flux) of planktic (green) and benthic (purple) foraminifera in numbers per cm^2 per ka. Roman numbers indicate Marine Isotope Stages (MIS) 1–5 and grey horizontal bars mark Heinrich events H1–H6

273x193mm (300 x 300 DPI)

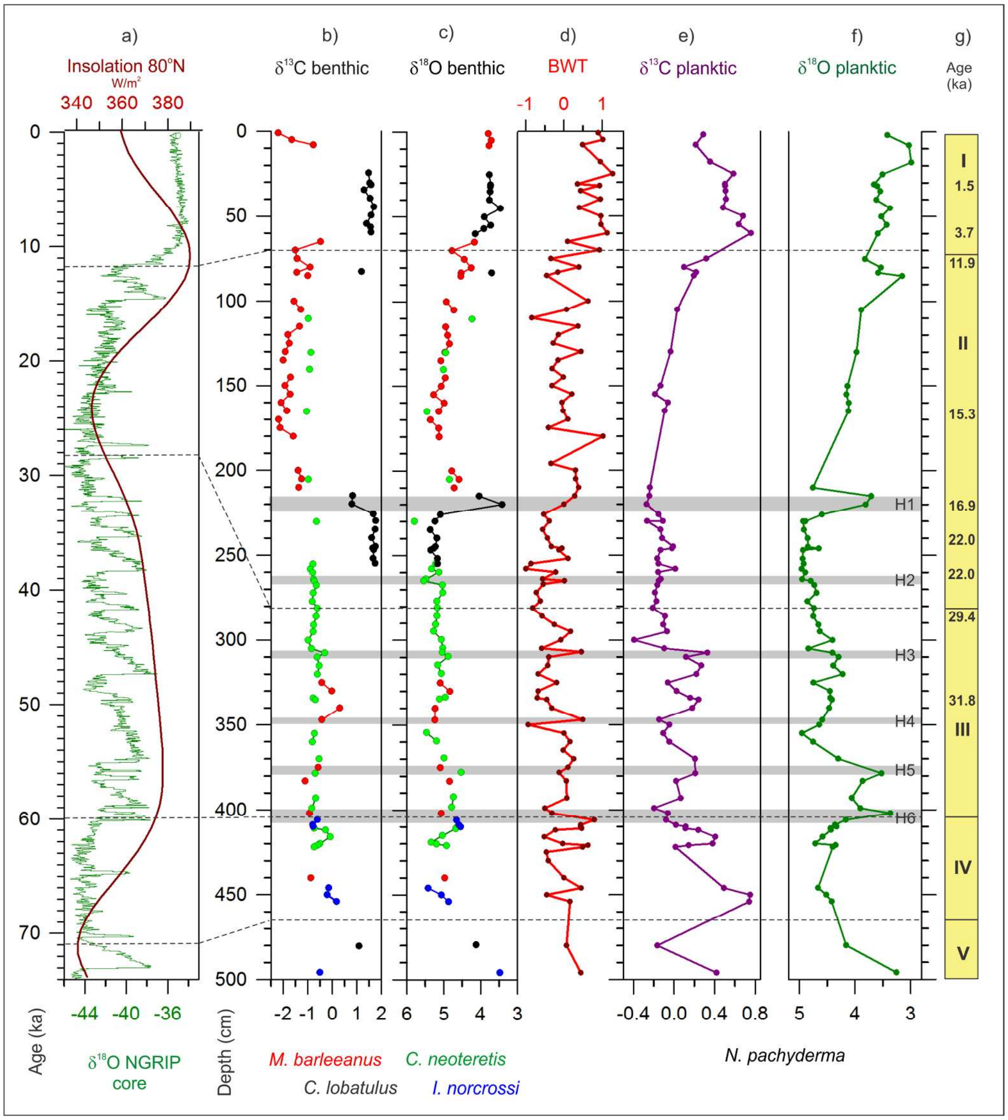

Fig. 7. Stable isotope data: a) δ^{18}O record of North Greenland Ice Core Project (NGRIP) (Svensson *et al*. 2008) and insolation curve at 80°N (Berger 1978); b) and c) δ^{13}C and δ^{18}O isotope records of core HH11-09GC, respectively based on the four benthic foraminiferal species; d) Calculated bottom water temperature (BWT) based on transfer functions; e) Planktic δ^{13}C and f) δ^{18}O records based on *N. pachyderma*; g) Calibrated ^{14}C ages in ka and Marine Isotope Stages (MIS) in Roman numbers. Grey horizontal bars mark the Heinrich events H1–H6.

199x221mm (300 x 300 DPI)

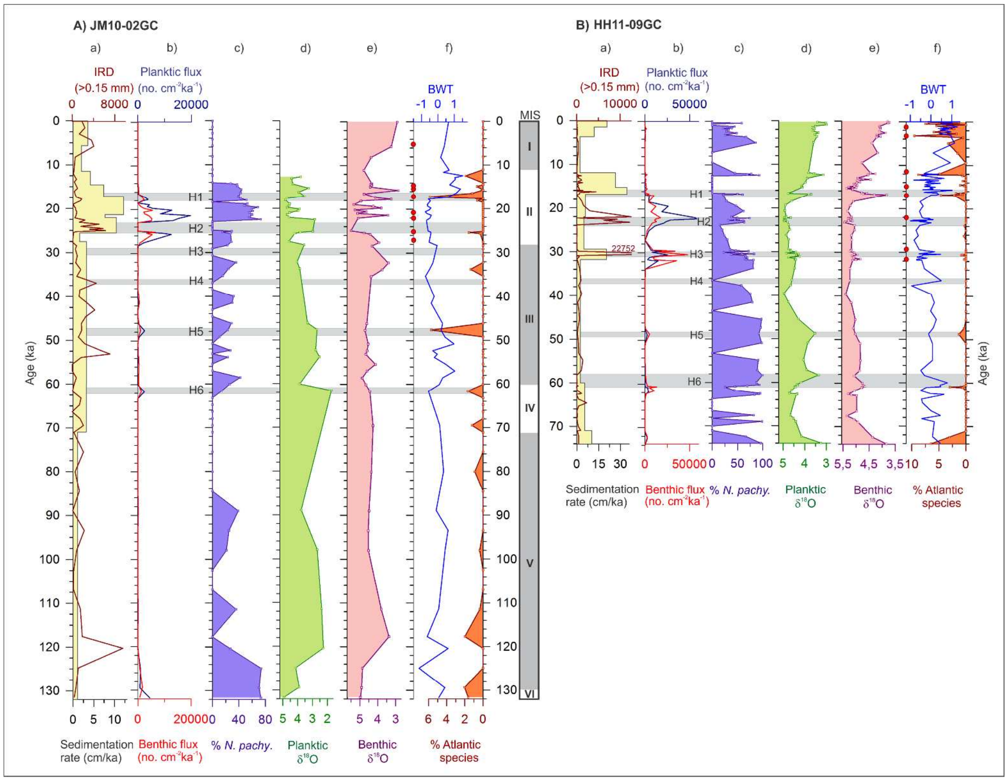

Fig. 8. The comparative logs of core JM10-02GC (Chauhan *et al.* 2014) A) and core HH11-09GC (this study) B). The same set of parameters has been presented for both cores: a) Sedimentation rate (cm/ka, yellow area) and concentration of IRD grains >150 µm (maroon line); b) Accumulation rates (flux) of planktic (blue) and benthic (red) foraminifera in numbers per cm^2 per ka; c) % *N. pachyderma*; d) and e) Planktic and benthic $\delta^{18}O$ isotope records, respectively; f) Bottom water temperature (BWT) calculated by transfer functions (blue) and % 'Atlantic species' group (orange). Red dots are calibrated ^{14}C ages (in ka) measured in both cores. Marine Isotope Stage (MIS) boundaries are marked in the column between A) and B). Grey horizontal bars mark Heinrich events H1–H6 in both panels.

338x261mm (300 x 300 DPI)

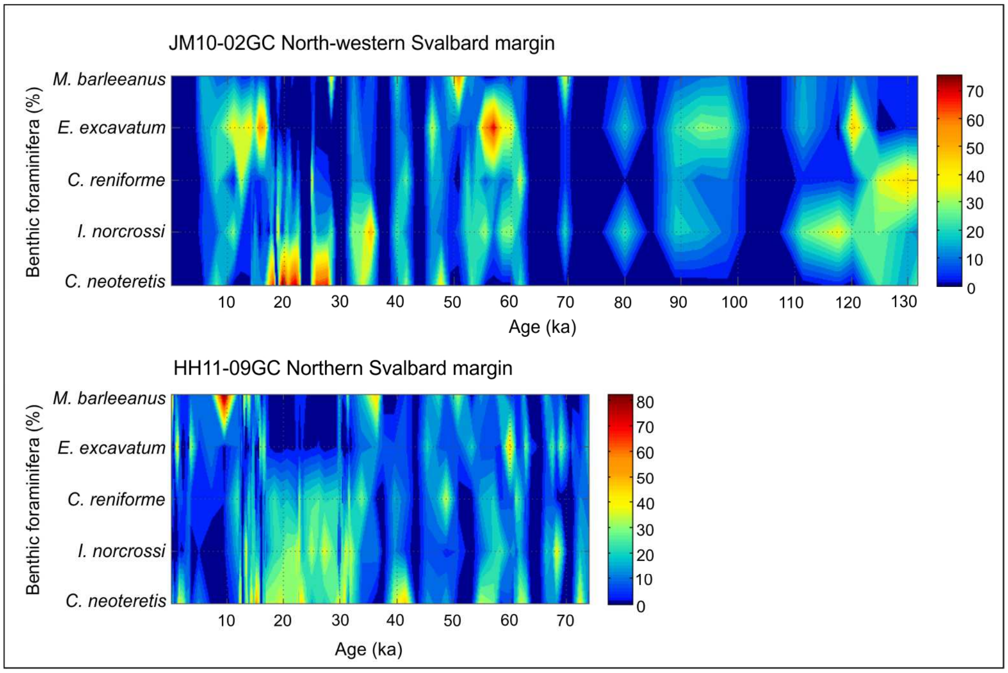

Fig. 9. Abundance of five dominant benthic foraminifera species (in %) in core JM10-02GC from the southern Yermak Plateau on the north-western Svalbard margin and in core HH11-09GC from the upper slope north of Nordaustlandet on the northern Svalbard margin. Dark blue region marks barren intervals.
178x118mm (300 x 300 DPI)

Figure Captions

Fig 1: A) Overview map of the Nordic Seas and the Arctic Ocean showing the location of Svalbard. B) Map of the northern Nordic Seas and the Barents Sea showing the main water masses, surface currents and oceanic fronts. C) Locations of the cores HH11-09GC (white circle) studied in this paper and the previously published sediment core JM10-02GC (open circle, Chauhan *et al.* 2014) on the northern Svalbard margin. Bathymetric map is from the International Bathymetric Chart of the Arctic Ocean (IBCAO) v3 (Jakobsson *et al.* 2012).

Fig 2: CTD (Conductivity, Temperature, Depth) profile from core site HH11-09GC taken on 9th September, 2011. Different water masses are labelled.

Fig. 3A: Scanning electron microscope (SEM) images of pristine benthic foraminifera used for radiocarbon dating and isotope studies: 1, 2. *Neogloboquadrina pachyderma* (sinistral); 3. *Cassidulina neoteretis*; 4. *Islandiella norcrossi*; 5, 6, 7, 8. *Cibicides lobatulus*; 9. *Astrononion gallowayi*; 10, 11, 12. *Melonis barleeanus*; 13. *Cassidulina reniforme*; 14, 15. *Nonionellina labradorica*; 16. *Elphidium tumidum*; 17. *Elphidium subarcticum*; 18, 19, 20. *Elphidium excavatum*; 21, 22. *Buccella* spp.; 23, 24. *Pullenia bulloides.*

Fig. 3B: Scanning electron microscope (SEM) images of dissolved (1–12) and pyritised foraminifera (14, 15). Number 13 shows digital image of silica spicules obtained from 7–8 cm and 50–60 cm core depth of core HH11-09GC. Number 14 and 15 show SEM images, elemental composition of mapped grey square area by Energy Dispersive X-ray Spectrometry (EDS) and digital image of two pyritised specimens. 1, 2. *Neogloboquadrina pachyderma* (sinistral); 3. *Cassidulina reniforme*; 4. *Cassidulina neoteretis*; 5. *Islandiella islandica*; 6, 7, 8, 9. *Melonis* *barleeanus*; 10. *Cibicides lobatulus*; 11. *Rupertina stabilis*; 12. *Nonionella turgida*; 13. Silica spicules; 14. *Parafissurina* sp.; 15, *Melonis barleeanus.*

Fig 3C: Scanning electron microscope (SEM) images of other benthic species present in core HH11-09GC (1–16) and benthic foraminifera from the 'Atlantic species group' (17–30) identified from core HH11-09GC and JM10-02GC: 1. *Cibicides wuellerstorfi*; 2. *Bulimina marginata*; 3. *Bulimina aculeata*; 4. *Trifarina fluens*; 5. *Trifarina angulosa*; 6. *Triloculina trihedra*; 7. *Millionella subrotunda*; 8. *Lagena striata*; 9. *Lagena gracillima*; 10, 11. *Ioanella tumidula*; 12. *Lenticulina* sp.; 13. *Oolina hexagona*; 14. *Stainforthia loeblichi*; 15. *Hyalinea baltica*; 16. *Pullenia osloensis*; 17, 18. *Eilohedra nipponica*; 19. *Triloculina oblonga*; 20, 21. *Anomalinoides minimus*; 22, 23. *Gyroidina umbonata*; 24, 25. *Sagrina subspinescens*; 26. *Valvulineria arctica*; 27. *Pyrgo williamsoni*; 28. *Pullenia subcarinata*; 29. *Eggerella bradyi*; 30. *Cibicides pachyderma*.

Fig. 4: Logs of the core HH11-09GC: a) Calibrated ^{14}C ages in ka; b) Lithological log; c) Boundaries and ages of Heinrich events (H1–H6) and meltwater pulse (mwp); d) Magnetic susceptibility; e) Green-red ('a') spectrum; f), g) and h) Concentration of IRD per gram dry weight sediment in three different size fractions (>1 mm, 0.5–1 mm and 0.15–0.5 mm, respectively); i) Planktic/benthic (P/B) ratio; j) Concentration of planktic (green) and benthic foraminifera (purple) in number per gram dry weight sediment; k) Insolation curve at 80°N (Berger 1978). Marine Isotope Stages (MIS) indicated by Roman numbers are defined based on Martinson *et al.* (1987).

Fig. 5: Age-depth plot, planktic $\delta^{18}O$ record and sedimentation rates for core HH11-09GC. Calibrated ages in years before present (yr BP) are shown with 1 sigma error bars. Numbers in the lower panel indicate sedimentation rate in cm/ka. Grey horizontal bar in the age-depth plot marks level with identical dates (no sedimentation rate calculated). Vertical dotted lines mark Marine Isotope Stages (MIS) 1–5, which are labelled with Roman numbers.

Fig. 6: a) to i) Relative abundance of most common benthic foraminiferal species. Panel i) also presents 'Atlantic species group' (see text for explanation); j) Relative abundance of planktic foraminiferal species: *Neogloboquadrina pachyderma* (sinistral) (violet), *Turborotalita quinqueloba* (green) and other planktic species (grey). Vertical bars mark barren intervals; k) Calibrated ^{14}C ages in ka; l) Accumulation rates (flux) of planktic (green) and benthic (purple) foraminifera in numbers per cm^2 per ka. Roman numbers indicate Marine Isotope Stages (MIS) 1–5 and grey horizontal bars mark Heinrich events H1–H6.

Fig. 7: Stable isotope data: a) $\delta^{18}O$ record of North Greenland Ice Core Project (NGRIP) (Svensson *et al.* 2008) and insolation curve at 80°N (Berger 1978); b) and c) $\delta^{13}C$ and $\delta^{18}O$ isotope records of core HH11-09GC, respectively based on the four benthic foraminiferal species; d) Calculated bottom water temperature (BWT) based on transfer functions; e) Planktic $\delta^{13}C$ and f) $\delta^{18}O$ records based on *N. pachyderma*; g) Calibrated ^{14}C ages in ka and Marine Isotope Stages (MIS) in Roman numbers. Grey horizontal bars mark the Heinrich events H1–H6.

Fig. 8: The comparative logs of core JM10-02GC (Chauhan *et al.* 2014) A) and core HH11-09GC (this study) B). The same set of parameters has been presented for both cores: a) Sedimentation rate (cm/ka, yellow area) and concentration of IRD grains >150 µm (maroon line); b)

Accumulation rates (flux) of planktic (blue) and benthic (red) foraminifera in numbers per cm^2 per ka; c) % *N. pachyderma*; d) and e) Planktic and benthic $\delta^{18}O$ isotope records, respectively; f) Bottom water temperature (BWT) calculated by transfer functions (blue) and % ‘Atlantic species’ group (orange). Red dots are calibrated ^{14}C ages (in ka) measured in both cores. Marine Isotope Stage (MIS) boundaries are marked in the column between A) and B). Grey horizontal bars mark Heinrich events H1–H6 in both panels.

Fig. 9: Abundance of five dominant benthic foraminifera species (in %) in core JM10-02GC from the southern Yermak Plateau on the north-western Svalbard margin and in core HH11-09GC from the upper slope north of Nordaustlandet on the northern Svalbard margin. Dark blue region marks barren intervals.

Tables

Table 1: Conventional AMS ^{14}C and calibrated ages for cores HH11-09GC and JM10-02GC.

Table 2: Ecology and taxonomy of most abundant planktic and benthic foraminiferal species in core HH11-09GC.